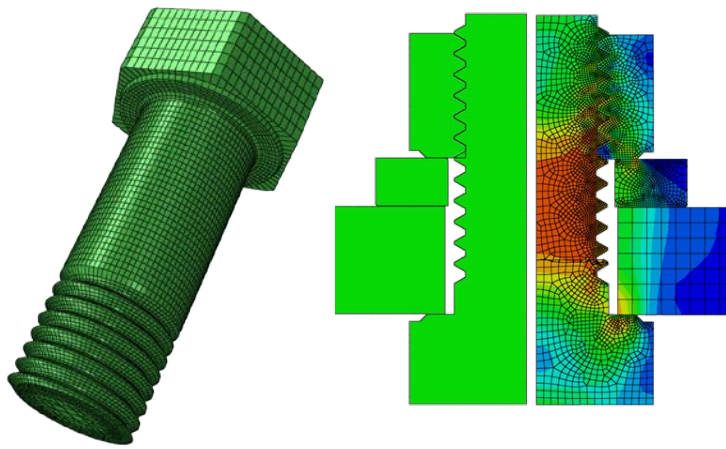




RESEARCH REPORT

VTT-R-01467-17



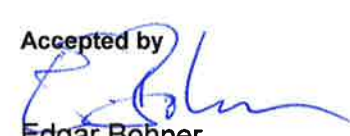


SIROCO

Report on numerical model calibration

Authors: Petr Hradil, Merja Sippola
VTT Technical Research Centre of Finland
Timo Manninen
Outokumpu Stainless Oy
Nancy Baddoo, Anqi Chen
Steel Construction Institute

Confidentiality: Confidential until June 2018

Report's title SIROCO: Report on numerical model calibration	
Customer, contact person, address European Commission	Order reference RFSR-CT-2014-00024
Project name Execution and reliability of slip-resistant connections for steel structures using CS and SS	Project number/Short name SIROCO
Author(s) Petr Hradil, Merja Sippola, Timo Manninen, Nancy Baddoo, Anqi Chen	Pages 70/
Keywords stainless steel, FEM, creep, relaxation, slip-resistant bolts	Report identification code VTT-R-01467-17
Summary <p>This report is part of the Work Package 5 "Preloading of stainless steel bolts" of SIROCO project, and therefore its focus is to develop a numerical model for slip-resistant connections made of stainless steel.</p> <p>Several options for the geometry, material models and calculation settings are analysed in the report and recommendations are given for the future use of finite element models to predict the long-term behaviour of stainless steel slip-resistant bolts.</p> <p>The material models are calibrated and validated against the experiments carried out in the SIROCO project (tensile tests, creep tests and relaxation tests) and recommended material parameters are provided which are valid for the steel grades used in the project.</p>	
Confidentiality	Confidential until June 2018
Espoo, 15.3.2017	
Written by  Petr Hradil Research Scientist	Reviewed by  Ludovic Fülöp Principal Scientist
	Accepted by  Edgar Bohner Research Team Leader
VTT's contact address P.O. Box 1000, FI-02044 VTT, Finland	
Distribution (customer and VTT) Project partners (pdf copy will be stored in the project workspace) European Commission	
<i>The use of the name of VTT Technical Research Centre of Finland Ltd in advertising or publishing of a part of this report is only permissible with written authorisation from VTT Technical Research Centre of Finland Ltd.</i>	

Preface

This report is part of the study (Work Package 5 of SIROCO project) to provide preloading levels and preloading methods for stainless steel slip-resistant connections taking into account the effect of material relaxation in bolt assemblies.

The aim of the report is to fulfil one of the targets of Work Package 5 to deliver “*Mathematical model for creep deformation and stress relaxation in stainless steel plate materials*”. Such mathematical model will be used in the finite element parametric study in Work Package 6, and therefore its suitability has to be verified on selected numerical models of the bolt assemblies in Task 5.5.

The particular goals of Task 5.5 are:

- development of numerical model of stainless steel bolt assembly including relaxation behaviour of plates and bolts presented in Chapters 2, 3 and 4 of this report
- calibration of the model against the test results in Chapter 7
- optimization of the model to provide good quality results with reasonable computational demands for Task 6.4 in Chapters 2 and 4
- development of script for automatic model generation in Chapters 5 and 6

The report provides the description of the numerical tools used to calibrate finite element models of pre-loaded stainless-steel bolt assembly. The focus is especially on the development of proper material models that can take into account material creep and relaxation in bolts and connected plates. Several alternative material models are presented and the material parameters are calibrated for the selected austenitic, ferritic and duplex stainless steel grades. The test results produced in Work Package 5 are used here to calibrate and verify the material models. The report also contains the description of modelling and simulation techniques used in the finite element calculations, and the basic overview of the plug-in developed to simplify the numerical analysis in a parametric study.

The authors would like to thank all SIROCO project partners for the valuable feedback and especially to Outokumpu Stainless Oy, Outokumpu Avesta AB and University of Duisburg-Essen for the experimental test results needed for the calibration of material models.

Espoo 15.3.2017

Authors

Contents

Preface.....	2
1. Introduction.....	5
2. Numerical models of stainless steel bolt assemblies.....	7
2.1 Basic model types.....	7
2.1.1 Axisymmetric shell model.....	7
2.1.2 Solid brick model created by revolution of 2D shape.....	8
2.1.3 Solid tetrahedron model created by revolution of 2D shape	9
2.1.4 Solid brick model created from mesh	9
2.2 Thread representation	10
2.2.1 Flat surface	10
2.2.2 Model of the thread geometry	10
2.3 Additional modelling assumptions.....	11
2.3.1 Mesh density.....	11
2.3.2 Boundary conditions	11
2.3.3 Pre-loading method.....	11
2.3.4 Loading sequence.....	12
2.3.5 Contact behaviour.....	13
3. Rate dependent material definition.....	14
3.1 Simple empirical relaxation model	14
3.2 Mixed kinematic and isotropic hardening model.....	17
4. Loading control	20
4.1 Iterative pre-tightening	20
4.2 UAMP subroutine.....	20
5. Models parametrization.....	21
5.1 Configuration file.....	21
5.2 Material definition.....	22
6. Graphical user interface.....	23
6.1 Abaqus plug-in for axisymmetric 2D bolt assembly	23
6.2 Abaqus plug-in for 3D connection with multiple bolts	24
7. Material behaviour	25
7.1 Material models for plates.....	25
7.1.1 Validation of Chaboche model in tension with different loading rates	25
7.1.2 Validation of Chaboche model in creep.....	29
7.1.3 Validation of Chaboche model in relaxation	32
7.2 Material models for bolts.....	34
7.2.1 Validation of time hardening model	34
7.2.2 Validation of strain hardening model	36
8. Connection behaviour	41
8.1 The effect of model geometry	41
8.2 The effect of preloading rate	43
8.3 The effect of re-tightening	44
8.4 Slip behaviour	46
8.4.1 Introduction.....	46

8.4.2	Static coefficient of friction	47
8.4.3	Preliminary validation of FE models (carbon steel).....	49
8.4.4	Summary	54
9.	Summary	55
	References.....	55
	Annex A: List of model parameters.....	57
	Annex B: Material library	61
	Annex C: Configuration file example.....	64
	Annex D: CREEP subroutine.....	66
	Annex E: UHARD subroutine.....	67
	Annex E: UAMP subroutine	68
	Annex F: Derivation of strain-hardening model.....	69

1. Introduction

Bolted connections are very convenient joining method in steel structures. They combine the advantages of simple assembly and disassembly, together with a high load-carrying capacity. Their performance can be further improved by appropriate pre-loading that will guarantee that the shear load is transferred through the friction surfaces rather than the contact between bolt shank and hole. Design of such connections from stainless steel can be challenging due to the viscoplastic behaviour of the material and there is no standardized design procedure for stainless steel slip-critical connections up to date. Despite of the concerns about the loss of preloading force, it was demonstrated that stainless steel preloaded bolts perform well under static and cyclic loading [1].

The bolted connections are very complex in terms of geometry and interactions between different components of the bolt assembly. Therefore, a large variety of numerical models exist to predict their behaviour from on the simple beam or shell elements to full solid models with detailed threads and contacts definitions [2]. Three-dimensional solid models can be in principle used to predict the behaviour of the assembly under any type of loading, but they are naturally the most computationally demanding choice.

Our task was to develop a numerical model that is practical for the use in parametric study and possible engineering applications in the future. Thus, the large part of this report explores the possible model simplifications in terms of reduced dimensionality (e.g. 2D axisymmetric models), number of elements (e.g. optimized meshing algorithms) and calculation time increments. At the same time, we strived to provide the accurate prediction of the creep and relaxation effect in stainless steel bolts and plates. This goal, however, resulted in rather complex material definitions that had to be implemented by Fortran user subroutines in Abaqus. It was impossible to provide generic material parameters within this task, but the calibration methods for the material models' parameters is presented in this report as well as the source code of the Fortran subroutines.

As the numerical calculations are more efficient nowadays, a large number of finite element studies of preloaded bolt assemblies have been reported recently. The main differences between them are usually in the preloading method. There are several ways of controlling the preloading process in numerical models. For instance, nut rotation (torque control) is used to study the localized effects of bolt tightening (friction and setting of the thread or local strains), but it requires detailed model of helical thread and use of an explicit solver allowing large deformations. Different preloading methods can be used when the role of the thread is not essential for the calculation such as initial stress or deformation, load or displacement control of the internal surfaces, or pre-heating. Another important issue is the choice of suitable element for the bolt. While most of the studies prefer hexahedral (brick) elements, the standard meshing algorithms do not usually allow their use in a complex 3D geometry with helical thread and hexagonal head. Then either the meshing algorithm needs to be developed for this specific purpose or tetrahedral elements can be selected. The most common finite element solvers are Abaqus Explicit, Abaqus Standard, Ansys and LS-Dyna.

Numerical models of pre-loaded bolts were for instance developed in the HISTWIN project [3]. They were solid 3D models with detailed thread geometry and the preload inserted by the rotation of the nut. The large deformations and complex interactions forced the models calculation by explicit solver. The amount of preload had to be calibrated individually because of the effect of plate bending. A similar problem is addressed also in our calculations due to the material relaxation during preloading. Another example of complex 3D model of the bolt assembly was developed at University of Duisburg-Essen [4]. Here, the bolt assembly was created parametrically in a similar way as in our models. However, the focus was to study large strains in localized areas of the thread resulting in too detailed mesh for the purposes of our calculations. More examples of finite element 3D models are presented in *Table 1*.

Table 1 Selected 3D FEM studies with preloaded bolts

Reference	preload method	FE solver	elements
Pavlović et al. [3]	nut rotation	Abaqus Explicit	4 nodes tetrahedron
Lorenz and Stranghöner [4]	nut rotation	Ansys	20 nodes brick
Ju et al. [5]	initial displacement	n/a	8 nodes brick
Bursi and Jaspart [6]	initial stress	Lagamine	8 nodes brick with incompatible modes
Krolo et al. [7]	initial displacement or initial stress	Abaqus Standard	8 nodes brick with incompatible modes
You and Zhou [8]	nut rotation	Abaqus Explicit	8 nodes brick with reduced integration
Izumi et al. [9]	nut rotation	Ansys	4 nodes tetrahedron
Hwang	nut rotation	LS-Dyna	4 nodes tetrahedron

¹⁾ loading/duration values and units can be specified by the user

2. Numerical models of stainless steel bolt assemblies

The finite element models presented in this report were developed to simulate the behaviour of the bolt assembly with preloaded stainless steel bolts. The calibration of the model geometry, contact behaviour and boundary conditions involved selecting and testing the suitability of several variants of the model or its particular parts. The goal was to propose the optimal solution to produce accurate results with the reasonable calculation time. The most important decisions were made about the model dimensionality (2D axisymmetric or full 3D model) and the representation of the threads (flat surface or full thread geometry). All options presented in this section are included in the Python script [10] (called “the script” in this report) developed for the purpose of the model calibration (Task 5.5) and the parametric study in Abaqus [11]. The script is able to create the finite element models automatically, execute the calculation and evaluate the results if requested. It uses Abaqus/CAE libraries [12] for most of the modelling tasks excepting the 3D mesh with helical thread that is generated directly in Python.

2.1 Basic model types

The simplest representation of the assembly would be with 2D axisymmetric elements. Such model is very small and fast to calculate. It was used for the simulation of relaxation of the preloading force due to material creep, setting and contraction of the connected plates. However, the 2D model is not sufficient for simulation of the slip load, and therefore we have developed two additional versions of 3D models. One type is generated by revolution of the 2D model shapes (bolt, nut and washer) and the second version can be created from parametrically generated mesh with accurate shape of helical thread and hexagonal nut and bolt head. The procedure is adapted from [14] and is upgraded to produce larger elements in the middle of the bolt shank.

Even though the 3D parametrically generated mesh (section 2.1.4, Figure 3) is the most accurate representation of the real bolt assembly, the calculation of its nodes and elements would need further development to create more optimized models with denser and coarser mesh in different parts and to avoid elements with large aspect ratios. Therefore we have selected the 3D model created by revolution of the 2D shape of the bolt, the nut and the washer (section 2.1.2, Figure 2) for the purpose of the future parametric study. The procedure for 3D parametrically generated mesh is included in the modelling script, but it is not an option in Abaqus plug-in and the script or the configuration file has to be called directly with the parameter `helix = True`.

2.1.1 Axisymmetric shell model

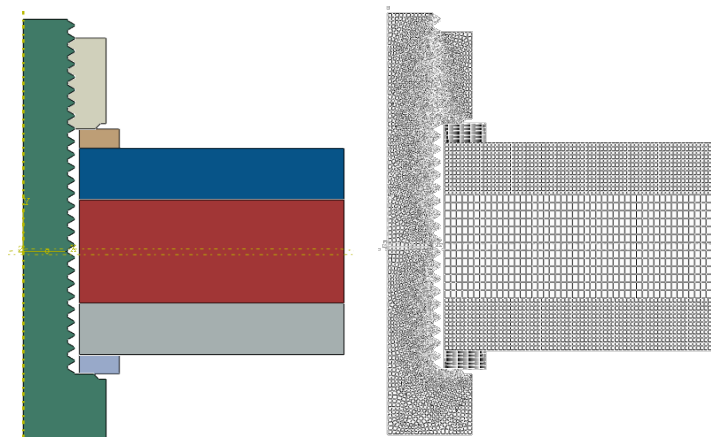


Figure 1. Example of 2D axisymmetric model and its mesh

Advantages:

- Small size of input file and output database
- Fast calculation
- Fast construction of the FE model
- Mesh generated automatically by Abaqus with the possibility to adjust its density near the contact surfaces and the corners

Disadvantages:

- Simplified cylindrical shape of the nut and bolt head
- Simplified thread (parallel rings)
- Limited only to one bolt
- Does not allow calculating slip of the plates

2.1.2 Solid brick model created by revolution of 2D shape

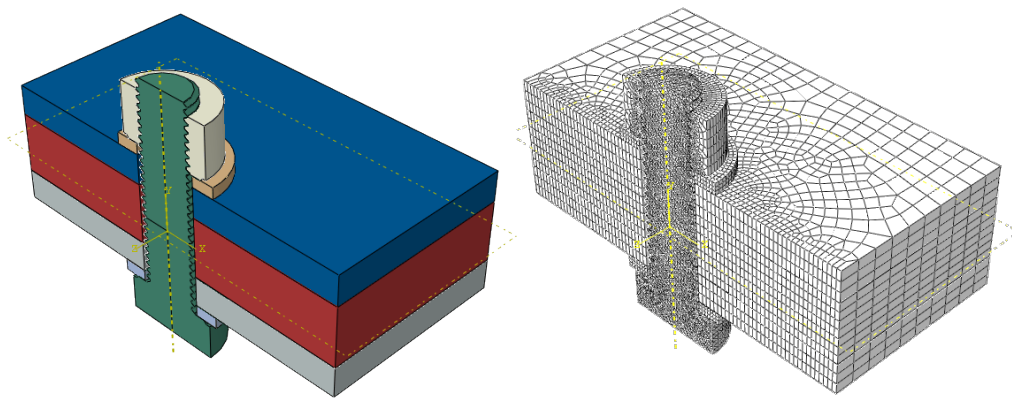


Figure 2. Example of 3D created by revolution of 2D shape and its mesh

Advantages:

- Possibility to calculate slip of the plates
- Possibility to have several bolts in a row
- Fast construction of the FE model
- Mesh generated automatically by Abaqus with the possibility to adjust its density near the contact surfaces and the corners

Disadvantages:

- Simplified cylindrical shape of the nut and bolt head
- Simplified thread (parallel rings)
- Large input file and output database
- Computationally demanding

2.1.3 Solid tetrahedron model created by revolution of 2D shape

This model is improved version of the previous one, where the selection of four node elements (tetrahedrons) allows further geometric modification by cutting the bolt head and nut to their exact shape.

Advantages:

- Possibility to calculate slip of the plates
- Possibility to have several bolts in a row
- Fast construction of the FE model
- Accurate hexagonal shape of the nut and bolt head
- Mesh generated automatically by Abaqus with the possibility to adjust its density near contact surfaces and the corners

Disadvantages:

- Simplified thread (parallel rings)
- Large input file and output database
- Higher number of elements than in brick model
- Computationally demanding

2.1.4 Solid brick model created from mesh

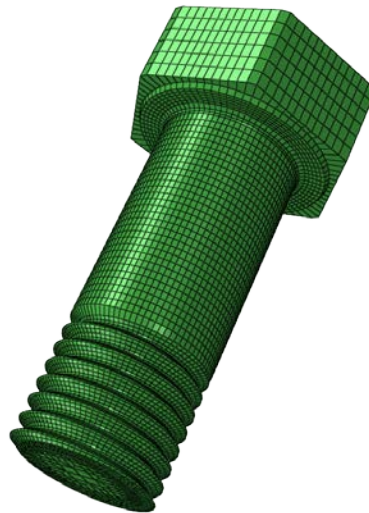


Figure 3. Example of 3D bolt with hexagonal head and helical thread created parametrically

Advantages:

- Possibility to calculate slip of the plates
- Possibility to have several bolts in a row
- Accurate hexagonal shape of the nut and bolt head
- Accurate helical thread

Disadvantages:

- Large input file and output database
- Slow construction of the FE model
- Mesh generated parametrically by Python script leading to a large number of elements
- Very slow and computationally demanding calculation

2.2 Thread representation

Two versions of thread representation in FE models were developed. One possibility is the flat surface (or line in 2D models) with the contact behaviour that will be calibrated later to match the deformation of the real thread. It can be generated in 2D axisymmetric models and 3D models created by revolution of 2D shape. Optionally it is possible to generate the real shape of the thread on the nut and the bolt models, where the contact surfaces are defined only on small areas that are normally compressed together during the bolt service life.

The original plan was to use flat surface (section 2.2.1, Figure 4) as the thread representation to save the computational time. We have selected the second, more geometrically accurate, model for the parametrical study (section 2.2.2) and we concentrated on eliminating the problems with its convergence. One of the greatest improvements of the convergence was loading of the model with deformation. Loading with deformation can be, however, difficult in some cases discussed in sections 2.3.3, 2.3.4 and 4 of this report.

2.2.1 Flat surface

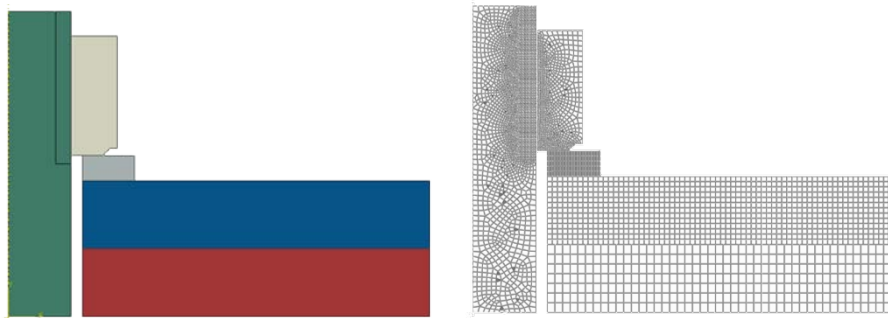


Figure 4. Example of flat thread representation and its mesh

Advantages:

- Only one straight contact face (or line in 2D models)
- Less convergence problems

Disadvantages:

- Need to calibrate the contact behaviour including the creep effects
- Inaccurate stress distribution in the threaded part of the bolt and the nut

2.2.2 Model of the thread geometry

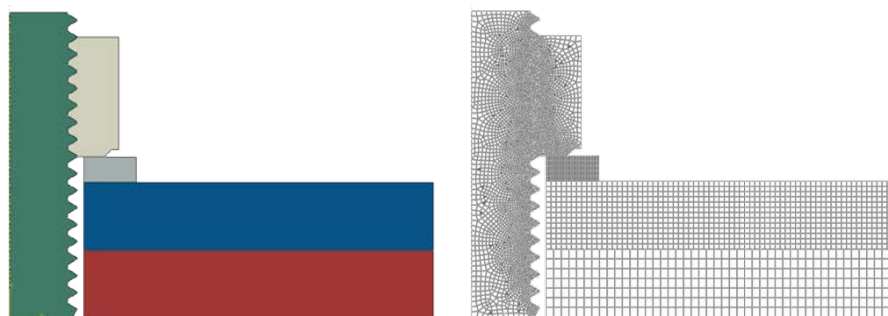


Figure 5. Example of full thread geometry and its mesh

Advantages:

- The contact behaviour can be rigid or simple friction without the need of creep calibration
- Accurate stress prediction around the threaded surfaces

Disadvantages:

- Many small contact faces
- Possible convergence problems

2.3 Additional modelling assumptions

2.3.1 Mesh density

The density of the mesh is defined in the script as the maximum distance between the nodes (in mm) in contact areas and outside of the contact areas. It is by default 0.6 and 0.15 mm respectively. The script, however, uses additional limits between those two values (e.g. for washers) or even coarser mesh (up to 4 times the larger value) for the plates to achieve more optimal mesh distribution in the whole model. The two input parameters should be then considered rather as approximate indicators of the mesh size.

2.3.2 Boundary conditions

Computational time can be greatly reduced by exploiting the symmetry planes in the model. It is assumed only one row of bolts in the studied cases, and therefore the vertical longitudinal symmetry plane (z-symmetry in the model) is always generated. Moreover, it is possible to simulate only the part of the bolt with the nut (disregarding the different behaviour of the bolt head) by activating the horizontal symmetry plane (y-symmetry) or in the case of single bolt it is also possible to have even smaller model with the vertical transverse symmetry plane (x-symmetry in the model). This option (Figure 6) is not present in the user interface and has to be used by calling the script directly or by the configuration file with the parameter `xSymm = True`.

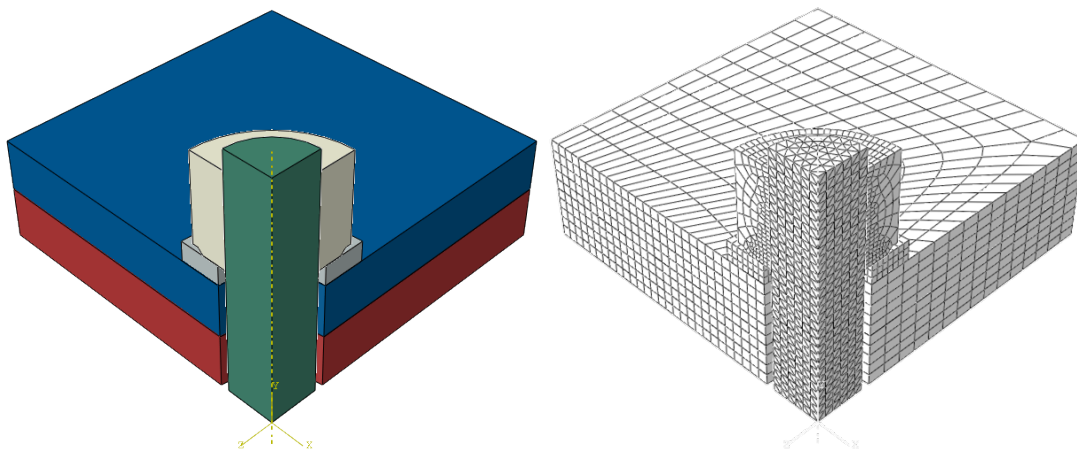


Figure 6. Example of 3D model with all 3 symmetry planes activated and its mesh

2.3.3 Pre-loading method

The script is able to create models with pre-defined loads in kN, MPa, % of the yield strength f_y (default option) or bolt shortening in mm, number of rotations of the nut, or degrees of rotation of the nut.

Several loading possibilities were briefly explored such as (a) simulation of nut rotation, (b) equivalent thermal loading, (c) initial contact overlapping or (d) initial stress field and (e) “bolt load” option from Abaqus/CAE. Rotation of the nut was successfully applied for instance in [4], but in our case it would mean that only 3D models will have to be used without any vertical symmetry planes. Initial contact overlapping was tested in the preliminary study made by SCI, but it does not allow further re-tightening of the bolt. The initial stress field was not tested at

all, because of the lack of the knowledge about the correct stress distribution. Therefore as the most suitable method was finally selected “bolt load” from all of the possible loading options.

The “bolt load” method in Abaqus/CAE is intended to model tightening forces or length adjustments in bolts or fasteners [15]. Adjusting the length is the preferred option because it has less convergence problems when used together with contacts. The most suitable internal surface for adjusting the bolt length is naturally the central plane where the stress distribution is assumed as uniform as possible. This method creates in practice standard boundary condition on this internal surface in the Abaqus input file (keyword *BOUNDARY) [16]. It means that the “bolt load” could be replaced by the equivalent boundary condition in symmetric cases (y-symmetry), where the central plane is not internal surface.

The problem arises when it is required to achieve a certain load (in kN, MPa or % of f_y) with the length adjustment of the bolt. The most common case is to require certain percentage of the yield strength in the bolt shank (e.g. 70% of f_y), but due to the nonlinear and strain rate dependent behaviour of the material it is not possible to accurately predict the corresponding deformation. An advanced method for controlling the load during the calculation had to be developed for this purpose and it is described in Section 4 of this report.

2.3.4 Loading sequence

The model should be flexible to simulate bolt assemblies that are pre-loaded in a relatively short time (usually a few seconds) and then left for many years to be able to observe material relaxation. In the case of multiple bolts, the script offers an option to load them in sequence or altogether in one step. The plates are laterally loaded after the tightening step(s) to create conditions necessary for slipping. This is followed by the relaxation period, where the bolts length are kept constant as well as the lateral load. This sequence of three or more steps can be repeated up to three times to simulate re-tightening of the bolt.

For example, *Table 2* shows the automatically generated loading sequence of the model with 2 bolts loaded to 70% of f_y and re-tightened after 10 years. The lateral load can be defined by the user for instance in kN (as in the *Table 2*) or in MPa. It is assumed that the slip loading will not be affected by material relaxation (therefore the step no. 4 is only 1 s long by default).

This assumption cannot be used in steps 2, 3, 6 and 7 where the correct duration is important because the material relaxation is very pronounced especially in the early stage already during pre-loading. As it was described in section 2.3.3, it is not possible to know the corresponding deformation if the load is specified in MPa or kN. In addition, because of the pre-loading speed is usually given as deformation per time (e.g. RPM), the exact duration of those steps is also unknown (see *Table 2*). Several solutions of this problem are presented in section 4.

Table 2 Example of the loading sequence

Step	Bolt 1 load	Bolt 2 load	Slip load	Duration
1 Initial	-	-	-	-
2 Tightening of bolt 1	growing to 70% of $f_y^{(1)}$	-	-	not known
3 Tightening of bolt 2	decreasing	growing to 70% of $f_y^{(1)}$	-	not known
4 Slip load	slightly decreasing	slightly decreasing	growing to 100 kN ¹⁾	1 s ¹⁾
5 Relaxation	decreasing	decreasing	100 kN	10 years ¹⁾
6 Tightening of bolt 1	70% of $f_y^{(1)}$	no load	100 kN	not known
7 Tightening of bolt 2	decreasing	70% of $f_y^{(1)}$	100 kN	not known
8 Relaxation	decreasing	decreasing	100 kN	40 years ¹⁾

¹⁾ loading/duration values and units can be specified by the user

2.3.5 Contact behaviour

The definition of the contact interaction properties will be performed in Task 6.4 especially for the shear planes between the connected plates. Therefore, the assumption for the contacts generated by the script was “hard” in normal direction and “rough” in tangential direction. However, the “penalty” option is suggested to use in the parametrical study as well as proper friction definition that will be defined in the Work Package 6.

3. Rate dependent material definition

3.1 Simple empirical relaxation model

A simple relaxation model was developed particularly for the bolt material that would be mostly subjected to relaxation during the service life of the joint. This strain hardening type model was fitted to relaxation tests of austenitic (grade 316), duplex (grade 2205) and lean duplex (grade 2101) cold drawn bars.

The target of this model development was a simple, few parameters relaxation model easy to fit for new steel grades and usable in the finite element program ABAQUS. A significant simplification was not including the effect of the strain rate in the pre-tightening phase and the assumption that the different pre-loading speed in real bolts would have only a minor effect on the final relaxation at the end of the service life. This is not necessarily always the case, but as the only test data available was at nearly constant and similar strain rates, including the effects of the preloading strain rate was not possible in this project. It would be necessary for modelling also creep situations, and it would be rather straightforward to add into the model if there were experimental results available.

The model is based on the relaxation tests at Outokumpu Avesta [13]. The inelastic part of deformation ε_i was assumed consisting of two parts, the time independent plastic strain ε_p and the time dependent relaxation/creep strain ε_v .

$$\varepsilon_i = \varepsilon_p + \varepsilon_v \quad (1)$$

The time independent plastic strain ε_p was derived from the tensile tests as the true stress - true plastic strain history and used in Abaqus input file with the *PLASTIC option. The time independent plastic behaviour from the experiments was used in tabular form in ABAQUS. It is also possible to fit the time independent plastic behaviour using one of the non-linear constitutive models. The model for the relaxation strain rate $\dot{\varepsilon}_v = d\varepsilon_v/dt$ assumes that while the total strain is constant in a relaxation test, the evolution of creep strain equals to the stress change caused by elastic deformation, i.e.

$$\dot{\varepsilon}_v = -\frac{1}{E} \dot{\sigma} = -\frac{1}{E} \frac{d\sigma}{dt} \quad (2)$$

According to Gupta and Li [17] and Hannula et al. [18], the natural logarithm of the creep strain rate in relaxation of stainless steels can be given by Eq. (3):

$$\ln \dot{\varepsilon}_v = (M/1 - M) \ln(t + a) + C \quad (3)$$

With different choice of constants () Eq. (3) can be given as Eq. (4)

$$\ln \dot{\varepsilon}_v = -b \ln(t + a) + \ln c \quad (4)$$

which leads to time-hardening form Eq. (5):

$$\dot{\varepsilon}_v = c(t + a)^{-b} \quad (5)$$

where the a , b and c are constant parameters that can be fitted experimentally and t is time. The material model may then take the strain-hardening form of Eq. (6) (see Appendix F):

$$\dot{\varepsilon}_v = c \left[\frac{\varepsilon_v(1 - b)}{c} + a^{1-b} \right]^{\frac{b}{b-1}} \quad (6)$$

In the current task, the strain-hardening model was used to reproduce the relaxation curve at any preloading level used in practice with austenitic steel bolts. Thus, the parameter c was calibrated as variable dependent on the initial stress σ_0 in the relaxation test according to Eq. (7):

$$c = c_1 \sigma_0^2 + c_2 \sigma_0 + c_3 \quad (7)$$

where c_1 , c_2 and c_3 are constant parameters fitted to the relaxation experiments. As it was empirically shown by Timo Manninen at Outokumpu Tornio, that under a certain threshold stress level (about $R_{p,0.1}$) the creep is negligible, a simpler linear fit was also used for the c parameter (see Eq. (8)).

$$c = c_4 \sigma_0 + c_5 \quad (8)$$

The curve fitting of the parameters to experimental relaxation results was carried out in Excel to the strain-hardening version of the model (Equation (6)). The Young's modulus used in the fitting to the relaxation test was the nominal value $E = 200$ GPa. The reason behind this choice was that the measured Young's modulus did not differ from the nominal value much in any other test with cold drawn material except for the 316 austenitic steel, and in that test the bars had not been straightened before testing, so the low modulus in that test was probably due to bending. This model was fitted to relaxation experiments of austenitic, duplex and lean duplex steels. The parameter sets that fit all the data best are shown in *Table 3* and *Table 4*.

Table 3. Parameters of strain hardening model of cold-drawn bars with parabolic approximation of coefficient c

Grade	a	b	$c_1 \cdot 10^{10}$	$c_2 \cdot 10^8$	$c_3 \cdot 10^5$
EN 1.4401 (316) austenitic	0.5229	1.0371	1.0011	-6.1588	1.7196
EN 1.4162 (2101) lean duplex	0.6010	1.0537	1.2623	-7.5340	2.0036
EN 1.4462 (2205) duplex	0.6253	1.0730	1.7776	-10.7294	2.2678

Table 4. Parameters of strain hardening model of cold-drawn bars with linear approximation of coefficient c

Grade	a	b	$c_4 \cdot 10^8$	$c_5 \cdot 10^5$
EN 1.4401 (316) austenitic	0.5262	1.0320	6.9332	-2.3727
EN 1.4162 (2101) lean duplex	0.6056	1.0533	8.9375	-3.1295
EN 1.4462 (2205) duplex	0.6360	1.0727	12.4983	-4.9743

The strain hardening model for bolts was implemented in Abaqus Finite Element software as a CREEP subroutine. The source code is given in the Annex D.

There are several possible choices for the constitutive model describing the gradual yielding and evolution time independent plastic strain ε_p (for instance [19], [20], [21], [22], [23] and [24]). The engineering value of total strain measured in tensile test ε_{eng} was fitted in this study to the two-stage Ramberg-Osgood model proposed by Mirambell and Real [22] that describes the stress-strain relation very accurately (Equations (9) and (10)).

$$\varepsilon_{eng} = \begin{cases} \frac{\sigma_{eng}}{E_0} + 0.002 \left(\frac{\sigma_{eng}}{\sigma_{0.2}} \right)^n & \text{for } \sigma_{eng} \leq \sigma_{0.2} \\ \frac{\sigma_{eng} - \sigma_{0.2}}{E_{0.2}} + \varepsilon^* \left(\frac{\sigma_{eng} - \sigma_{0.2}}{\sigma_u - \sigma_{0.2}} \right)^m + \varepsilon_{0.2} & \text{otherwise} \end{cases} \quad (9)$$

$$\varepsilon^* = \varepsilon_u - \varepsilon_{0.2} - \frac{\sigma_u - \sigma_{0.2}}{E_{0.2}}, \quad \varepsilon_{0.2} = \frac{\sigma_{0.2}}{E_0} + 0.002 \quad \text{and} \quad E_{0.2} = \frac{E_0}{1 + 0.002n \left(\frac{E_0}{\sigma_{0.2}} \right)} \quad (10)$$

with the initial modulus of elasticity E_0 can be conservatively assumed to be 200 GPa, 0.2% proof stress $\sigma_{0.2}$, ultimate stress and strain σ_u and ε_u , and nonlinear parameters n and m curve-fitted to the experimental results of tensile tests (engineering stress σ_{eng} and engineering strain ε_{eng}). Then the strain shall be converted to true plastic strain according to Equation (11):

$$\varepsilon_p = \ln(1 + \varepsilon_{eng}) - \frac{\sigma_{eng}(1 + \varepsilon_{eng})}{E_0} \quad (11)$$

The results of constitutive model calibration are in *Table 5*.

Table 5. Parameters of constitutive model for time independent strain

Grade	$\sigma_{0.2}$ (MPa)	σ_u (MPa)	n	m	ε_u (%)
EN 1.4401 (316) austenitic	748.5	953.3	2.18	9.76	2.08
EN 1.4162 (2101) lean duplex	769.8	987.5	4.02	4.34	2.15
EN 1.4462 (2205) duplex	837.9	989.3	3.65	15.18	2.74

3.2 Mixed kinematic and isotropic hardening model

An extensive literature study revealed that room temperature creep and stress relaxation behaviour of stainless steel shows that following features:

- A. There exists a limiting stress value for the creep deformation. No creep occurs below the limit stress.
- B. The rate of creep deformation is a function of the overstress between the current stress and the creep limit.
- C. The creep limit increases due to work hardening during plastic deformation.
- D. The amount of creep deformation observed in creep tests depends on the loading rate used in the loading stage in the beginning of the test.
- E. The rate of creep deformation is closely related to the rate of work hardening in the material. Higher work hardening rate results in swifter deceleration of creep deformation.
- F. There is not difference between work hardening by creep test and work hardening in tensile testing. In spite of different deformation processes, the material strain hardens by equal amount as long as the plastic strain is the same.
- G. The creep deformation causes the yield surface to undergo kinematic hardening with insignificant amount of isotropic hardening. This observation holds in creep testing of annealed materials with relative low stress levels in vicinity of the 0.2% proof stress.
- H. No signs of secondary creep have been observed in room temperature testing.

Non-standard tensile tests with different constant loading rates in the range from 10^{-7} (1/s) to 10^{-2} (1/s) were carried out in order to investigate the plastic and viscoplastic behavior of all four plate materials. The results confirmed that the material response follows the theory of viscoplasticity based on overstress. It was also found that the viscosity function can be accurately described with the power law

$$\dot{\varepsilon}_p = \left\langle \frac{\sigma - \sigma_{th}}{D} \right\rangle^n \quad (12)$$

where σ is the current Cauchy stress in the sample, σ_{th} is the current creep limit. The creep limit is a function of cumulated plastic strain. D and n are material parameters. The notation $\langle \cdot \rangle$ denotes the MacCauley brackets

$$\langle x \rangle = \frac{1}{2} (x + |x|) \quad (13)$$

The features A-H and our own experimental results on the plastic and viscoplastic behavior define basic requirements for the constitutive model for the plate materials.

Based on a review of present state of the art in computational viscoplasticity, a constitutive model known as the Chaboche model was chosen for modelling the creep of plate materials. The Chaboche model is widely used both in academia and in industry for modelling cyclic plasticity. Furthermore, this model has been successfully used for modelling room temperature stress relaxation of AISI 316 type austenitic stainless steel.

The Chaboche model is a unified model. The immediate and time dependent plastic deformations are treated as one inelastic strain component. The time-independent plasticity is obtained as a limiting case. The model uses two internal state variables for describing the material hardening behaviour. One internal state variable is a tensorial back-stress α used for describing kinematic hardening of the material. The other state variable R accounts for isotropic hardening. Parametrized evolution laws are given for each internal variable. The back-stress is commonly described as a sum of components $\alpha^{(i)}$

$$\alpha = \sum_{i=1}^N \alpha^{(i)} \quad (14)$$

Parametrized evolution laws are given for each internal variable. The evolution of kinematic hardening components is described by

$$\dot{\alpha}^{(i)} = \frac{2}{3} C_i \dot{\epsilon}^p - \gamma_i \alpha^{(i)} \dot{\epsilon}^p \quad (15)$$

where N is the number of kinematic hardening components, $\dot{\epsilon}^p$ is the rate of plastic strain tensor and $\dot{\epsilon}^p$ is the equivalent plastic strain. C_i and γ_i are material parameters. The scalar isotropic hardening component R follows the evolution law

$$\dot{R} = b(Q - R) \dot{\epsilon}^p \quad (16)$$

The rate of equivalent plastic strain is given by the power law viscosity function

$$\dot{\epsilon}^p = \left\langle \frac{\|\sigma - \alpha\|_{VM} - R - k}{D} \right\rangle^n \quad (17)$$

where D , k and n are material parameters. The norm $\|\cdot\|_{VM}$ denotes the Von Mises yield function. The MacCauley brackets $\langle \cdot \rangle$ guarantee that there exists an elastic limit below, where no inelastic deformation occurs. The elastic limit also denoted the threshold for the onset of creep deformation and the limit at which stress relaxation ceases.

In the Chaboche model, the observed hardening behaviour is divided into kinematic and isotropic parts. Therefore, identification the material parameters for this model typically requires tests in which the direction of loading is reversed such as tension-compression tests. This kind of testing has not been carried out in Work Package 5. However, it is well known that the transition from purely kinematic hardening to combined isotropic and kinematic hardening takes place near 1% plastic strain in most engineering materials. Therefore, it can be assumed that the rate independent hardening is purely kinematic hardening until the transition point at 1% plastic strain.

In the present application, the inelastic strains are expected to remain well below the transition point. The constitutive model was nevertheless extended to yield realistic prediction for the material behaviour over the whole range that can be experimentally investigated with uniaxial tension tests. This will provide stable numerical calculation also in the possible case that a high stress concentration might occur in a localized region in the finite element model. Furthermore, this will also enable numerical experiments with hypothetical cold-worked plate materials.

After the transition point at 1% of plastic strain, the observed hardening was divided using a constant ratio X/Y in kinematic hardening and isotropic hardening components. For single phase plate materials 1.4003 and 1.4404 it was assumed that the hardening consists of 60% of kinematic hardening and 40% of isotropic hardening following the experimental findings of Feaugas. For the dual phase materials 1.4162 and 1.4462, it was assumed that the hardening is purely isotropic after the transition point

A numerical method was developed for identifying the parameters of the Chaboche model based on the results of extensive materials testing carried out in Task 5.2. The identification method has three stages:

- I. Identification of the parameters D and n in the viscosity function in Equation (17). The 0.2% proof stress values measured in tensile tests conducted with different constant loading rates in the range from 10^{-7} (1/s) to 10^{-2} (1/s) are used for the identification.
- II. Identification of the hardening parameters in Equations (14), (15) and (16). The true stress vs. logarithmic plastic strain curves measured in tensile tests conducted with different constant loading rates in the range from 10^{-7} (1/s) to 10^{-2} (1/s) are used for identification. The rate-dependent part of stress can be subtracted from the stress response using the viscosity function.
- III. Fine tuning the viscosity function by means of creep test curves. The viscosity function is fine-tuned in the range $\dot{\epsilon} < 10^{-7}$ using the results of constant load creep tests.

The developed numerical method was used to determine the Chaboche model for all four-plate materials. The identified material parameter are summarized in *Table 6* and *Table 7*.

Table 6. Backstress components of kinematic hardening

Grade	C_1 (MPa)	γ_1	C_2 (MPa)	γ_2	C_3 (MPa)	γ_3
EN 1.4404 (316L) austenitic	45949	591.4	617031	6765.3	1434	2.5
EN 1.4003 (410L) ferritic	623733	5855.1	17430	558.6	1680	10.8
EN 1.4462 (2205) duplex	947349	11334.6	252038	1222.1	2971	60.0
EN 1.4162 (2101) lean duplex	483769	4875.7	102445	975.3	6766	180.8

Table 7. Parameters of Chaboche model

Grade	D (MPa)	n	Q (MPa)	b	k (MPa)
EN 1.4404 (316L) austenitic	110	15.0	380	2.5	73
EN 1.4003 (410L) ferritic	130	11.0	104	10.8	106
EN 1.4462 (2205) duplex	313	24.3	723	2.8	106
EN 1.4162 (2101) lean duplex	329	30.2	649	3.5	109

The Chaboche model is not available in the Abaqus finite element software used as the modelling tool in Tasks 5.5 and 6.4 in the form described above. Therefore, the model was implemented in Abaqus as a UHARD user subroutine. The implementation was validated using reference cases. The source code is given in the Annex E.

4. Loading control

The sections 2.3.3 and 2.3.4 presented the basic modelling assumptions for the load implementation and the problem of predicting the required deformation of the bolt if the model has to reach certain preloading force or stress in the shank. The most convenient way would be to force the solver to interrupt the calculation at a certain point defined by the stress in the bolt. This issue could not be solved by conventional methods offered by Abaqus, and therefore we had to introduce two approaches to control the loading during pre-tightening steps. Both methods start the calculation with a certain total deformation request that should be larger than the real deformation at the desired pre-loading level. For this purpose, the shortening of the bolt assembly is calculated in the script using ideally elastic behaviour of all components. This estimation is then multiplied by so-called “overload” factor. It is recommended that this “overload” factor is at least 2 for nearly elastic applications without significant relaxation (such as carbon steels) and at least 4 for more non-linear material behaviour (e.g. stainless steels). The first method using iterative calculation (section 4.1) was abandoned because of its excessive time demands especially in the cases with re-tightening of the bolt. It was replaced by faster, more flexible, but slightly less accurate UAMP subroutine (Section 4.2, Annex F).

4.1 Iterative pre-tightening

This method is based on the post processing of the partly solved model with the last recorded pre-tightening step. The output database is automatically analysed and if the desired stress was reached in the bolt, the accurate deformation is calculated by interpolation between two neighbouring increments. Then the calculation has to be restarted with the corrected deformation request. If the desired stress was not reached, the calculation is also restarted, but with double “overload” factor. Then the required stress level is reached in all cases eventually.

Advantages:

- Correct value of desired stress also in the cases when the “overload” factor was underestimated
- Accurate loading value due to the interpolation between two increments

Disadvantages:

- Extremely long calculation time due to several model re-submissions
- Procedure for more bolts loaded at the same time is not yet developed

4.2 UAMP subroutine

Abaqus offers to control the step length also internally by defining the user amplitude in UAMP (or VUAMP) subroutine. The subroutine is able to conclude the step if a nodal variable (called sensor) reaches a certain value. Since the stress is calculated as element output, it could not be used directly. The stress prediction is therefore based on the reaction force in the vertical direction “RF2” in the loaded area of the bolt shank divided by the area of the neighbouring element faces. The source code of UAM subroutine is in Annex F of this report.

Advantages:

- Standard calculation time because the stress is evaluated at every increment
- It is possible to use the same subroutine on multiple bolts with different parameters

Disadvantages:

- Calculation continues to the next step even when the desired load was not reached
- The step is concluded at the first iteration with higher stress than the desired value and this can create some inaccuracy if the increments are too large

5. Models parametrization

The goal was to develop a procedure for generating fully functional numerical models of stainless steel bolt assemblies or simple structural details. Such models should cover the whole range of assembly shapes and sizes, and the materials used for the bolt, nut, washer and connected plates. We have also included the standard assembly systems used for carbon steel bolts (HV, HR) and carbon steel grades. As a result, the models are based on a large number of parameters. Therefore, we have implemented several measures to simplify the use of the script:

- (A) **Default values** – all of the parameters have a default value. Therefore, a fully functional model is always created even if there is no parameter provided.
- (B) **Libraries of standard parameters** – most of the particular material properties and dimensions can be obtained from the libraries or specified by the user. The libraries cover (a) materials used in the Eurocodes, (b) assembly systems or (c) standard bolts, nuts, washers and hole sizes. If the element from the library is selected, some of the default parameters are not necessary anymore. The standards used in the script are listed in *Table 8*.
- (C) **Configuration file** – is created each time the script is executed. It helps the user to recover or modify the previous calculations. More information is given in Section 5.1.
- (D) **Graphical user interface** – GUI can be used to quickly modify the default model parameters or re-launch the calculation from the configuration file. More information is given in Section 6.

Table 8 Standards used in the calculation script

Standard	Description	Implementation	
EN ISO 4014	bolt geometry	values are part of the script code	
EN ISO 4017			
EN ISO 4032	nut geometry		
EN 14399-3	bolt & nut geometry		
EN 14399-4			
EN 14399-5			
EN ISO 7091	washer geometry		
EN ISO 7093-1			
EN 1993-1-1	material properties		values are in text file and can be modified by the user
EN 1993-1-4			

5.1 Configuration file

The configuration file is created each time the script is executed and contains the list of model parameters. The variable names, their values and descriptions are listed in a systematic way in the configuration file. The example of the configuration file content is in Annex C of this report.

5.2 Material definition

The goal was to provide a simple definition of the possible materials used in the numerical models. Those materials should include the common carbon steel and stainless steel grades with different level of complexity depending on the available material parameters. The database of pre-defined materials suitable for the plates or other parts of the assembly is stored in the "material.txt" file. Abaqus plug-in, the script or the configuration file can directly refer to the material names in this database. All material model types are identified by 3-letters code followed by the list of material parameters. For instance, *ELA*, 220 stands for the ideally elastic material with the modulus of elasticity 220 GPa.

The simplest definition of plasticity is ideally plastic material (in true stress-strain terms) that is defined by the modulus of elasticity followed by the yield strength in MPa. For instance *PLA*, 200, 290 is the definition of 1.4439 grade stainless steel and it can be generated by requesting "1.4439" or its alternative designations such as "317LMN" or "S31726". If the ultimate strength and uniform elongation of the material is known, this ideally plastic material definition can be extended to so-called bi-linear material (*BLN*) with those two parameters added to the list respectively. Unfortunately, the uniform elongation is not usually provided in the design standards, and therefore such materials are not included in the default database.

The following group of material models are non-linear materials, commonly called Ramberg-Osgood type materials. The database includes the possibility to define the materials with the parameters of models by Holmqvist and Nadai (*HNA*) [19], Hill's modification of Ramberg-Osgood material (*SRO*) [20][21], and their variants by Mirambell and Real (*MRO*) [22], Rasmussen (*RRO*) [23], and Gardner (*GRO*) [24]. Most of the stainless steel grades in EN 1993-1-4 [25] include all the parameters needed for at least Ramberg-Osgood's model. For instance, *SRO*, 220, 280, 7, 450 is the definition of 1.4003 grade (or 3Cr12, S41003, S40977, 409L) with modulus of elasticity 220 GPa, 0.2% proof strength 280 MPa, nonlinear factor 7 and the last optional parameter, the ultimate strength 450 MPa. Those materials are transformed to true stress-true plastic strain form when used in the numerical model.

All of the materials mentioned in the previous paragraphs are based on the simple definition of metal plasticity that is independent on the strain rate, and therefore not able to simulate creep and relaxation of the model parts. Our goal was to develop more complex rate-dependent materials (described in section 3), and therefore it should be possible to include them in the database. The mixed isotropic and kinematic hardening rule based on Chaboche material model is for instance identified by *UHA* followed by the modulus of elasticity, the yield strength, number of back-stresses, initial stress, back-stress parameters and all remaining parameters required by the *UHARD* subroutine. A different set of parameters is recommended for the plates and washers, and for the bolt and the nut.

The complete list of pre-defined materials and their parameters is in Annex B of this report.

6. Graphical user interface

The graphical user interface (GUI) to control the script was developed in order to increase the efficiency of the common tasks performed with the script and to enable project partners and other users quickly generate FE models. The large amount of possible model parameters resulted in the development of two different user interfaces, one for 2D axisymmetric models and the second one for 3D assemblies with the possibility to simulate more bolts in a row and slip loading. Both GUIs execute the same script with pre-selected parameters that are relevant for the particular situation and the parameters defined by the user in their controls.

Both basic interfaces offer the option to submit the job on the local computer or to create just model including generated input file. If the job is submitted, it will be monitored and after its completion, the results will be extracted to CSV file readable by most spreadsheet editors. If the job is submitted manually (e.g. using remote server), the results can be still evaluated by selecting “Evaluate results” in the plug-in drop-down menu and then the appropriate ODB database of Abaqus results (see Figure 7).

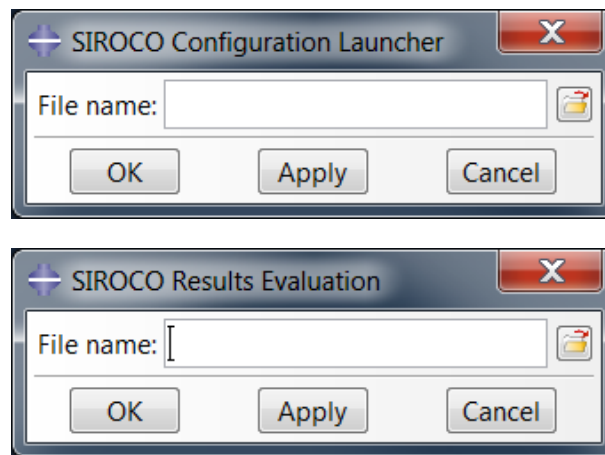


Figure 7 Configuration file launcher and results evaluation GUI

Since the execution of the script generates automatically a configuration file with all its parameters, the additional dialog box was created to simply re-submit the existing (or manually edited) task (see Figure 7).

6.1 Abaqus plug-in for axisymmetric 2D bolt assembly

The plug-in for 2D axisymmetric bolts (see Figure 8) has pre-defined dimensionality ($mDim=2$), and disabled vertical symmetry ($ySymm=False$). The definition of loading sequence contains only options for pre-tightening and relaxation, because the slip loading is not possible in axisymmetric models.

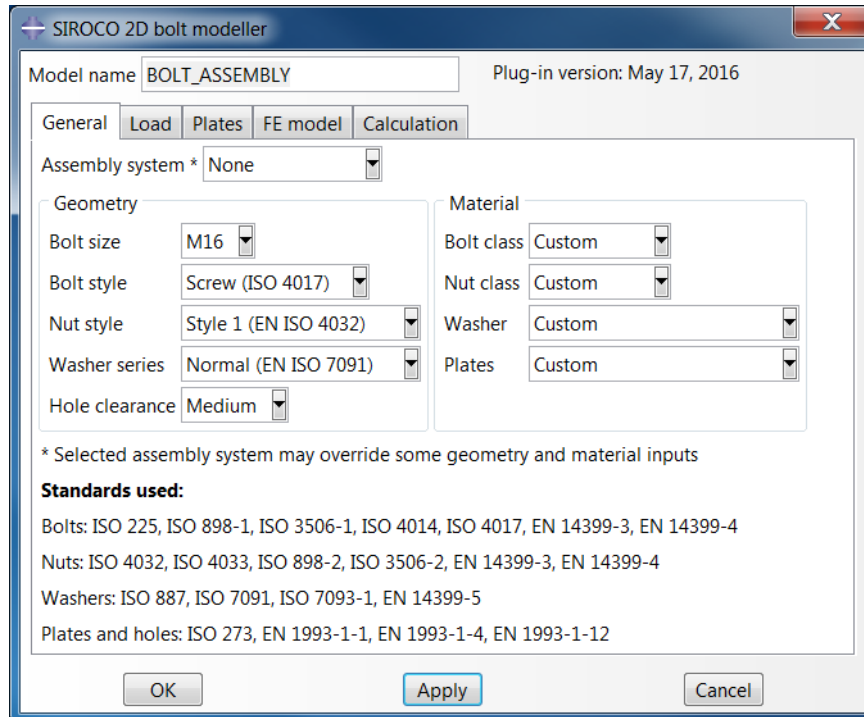


Figure 8. The basic user interface for creating 2D bolts

6.2 Abaqus plug-in for 3D connection with multiple bolts

The plug-in for 3D bolt assemblies (see Figure 9) has pre-defined dimensionality ($mDim=3$), and option to select vertical symmetry ($ySymm$). The definition of loading sequence contains pre-tightening, slip and relaxation. Additionally, it is possible to simulate several bolts in a row and define their internal spacing. The default parameters are defined to create a model of standard creep test of two M16 bolts in a row.

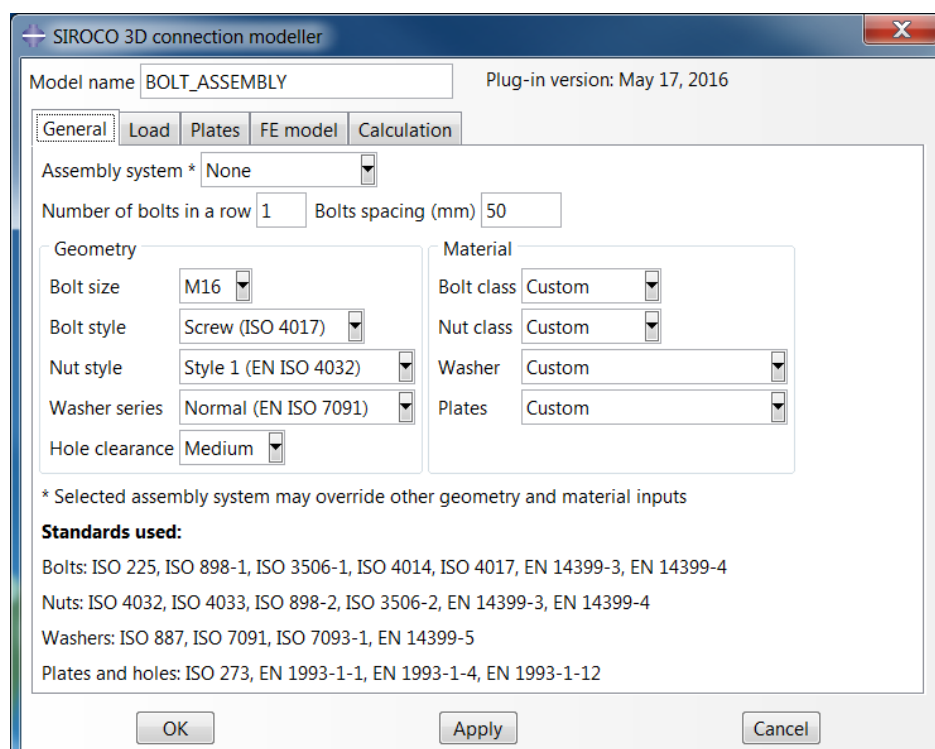


Figure 9. The basic user interface for creating 3D connections

7. Material behaviour

7.1 Material models for plates

7.1.1 Validation of Chaboche model in tension with different loading rates

The results of tensile tests of coupons from austenitic steel plates EN 1.4404 (316L) tested in Task 5.1 of SIROCO project were reproduced using the calibrated material model from Chapter 3.2 on single finite element. The boundary conditions were selected in such a way that the von Mises stress was equal to the principal stress in the axial direction of this element. Similarly, the equivalent plastic strain is identical to the plastic strain in the loading direction. The stresses and strains were then recalculated to their engineering values and their relation is presented in Figure 10 to Figure 15.

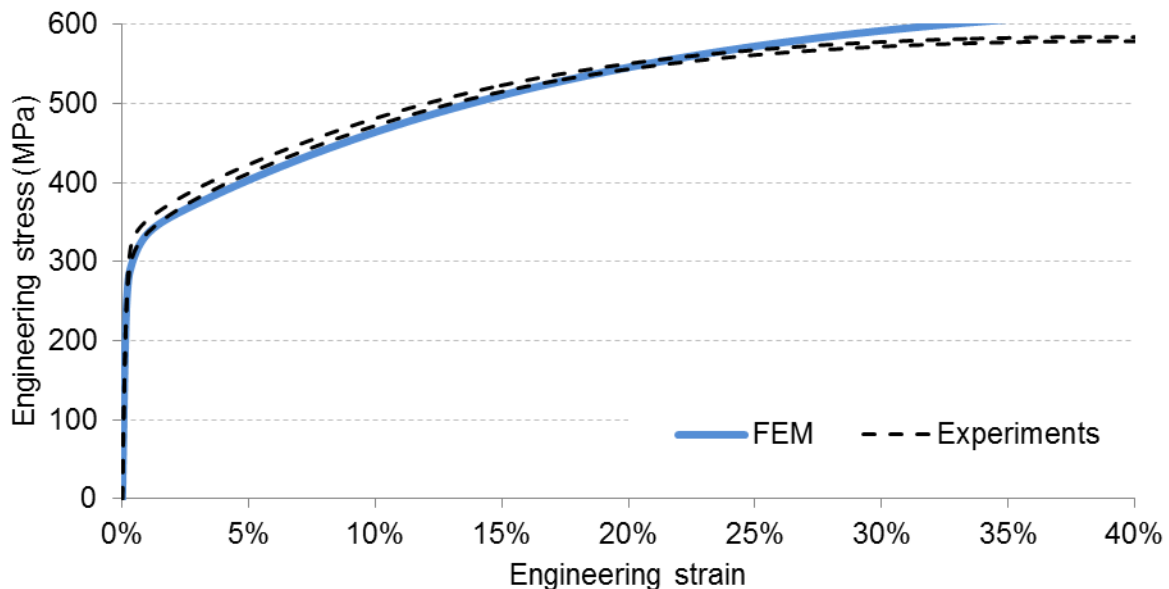


Figure 10. Verification of the material model in tension at constant strain rate $1 \cdot 10^{-2} \text{ s}^{-1}$

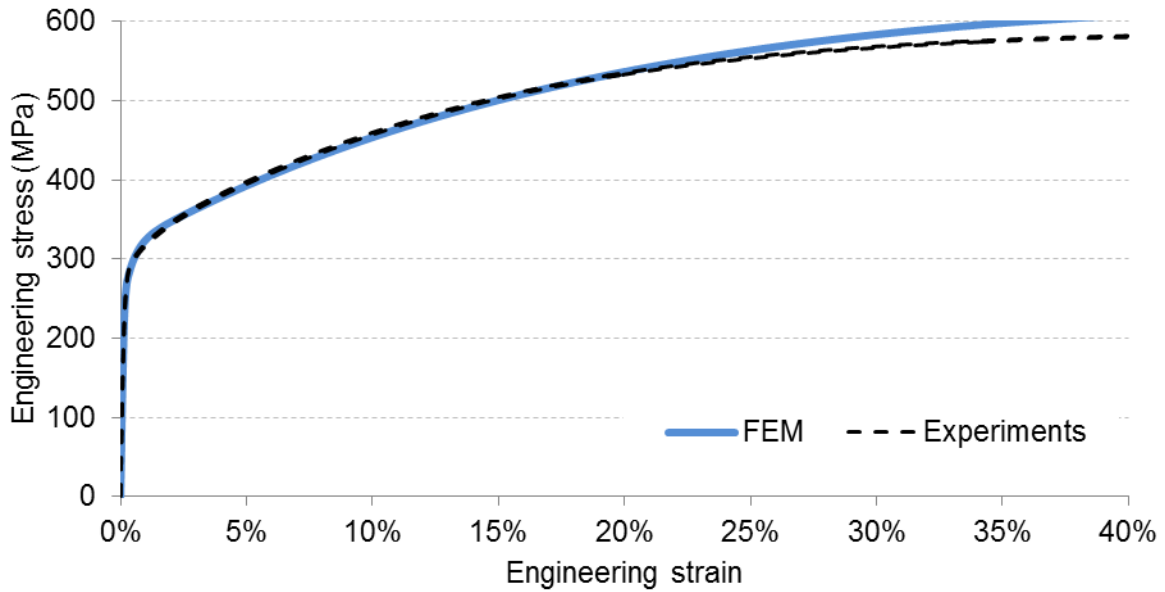


Figure 11. Verification of the material model in tension at constant strain rate $1 \cdot 10^{-3} \text{ s}^{-1}$

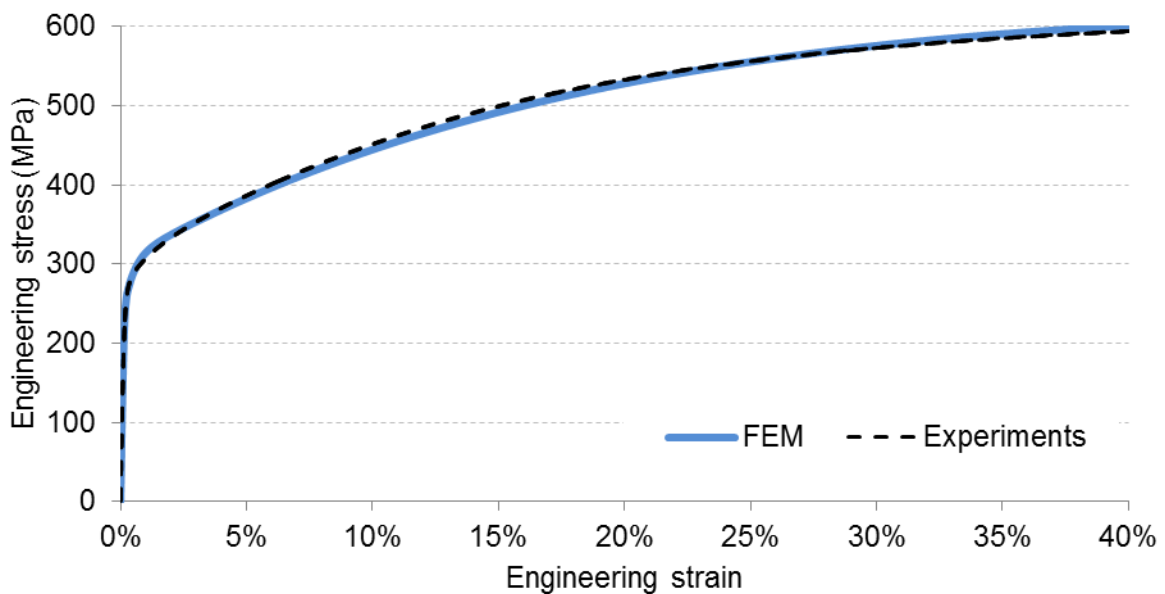


Figure 12. Verification of the material model in tension at constant strain rate $1 \cdot 10^{-4} \text{ s}^{-1}$

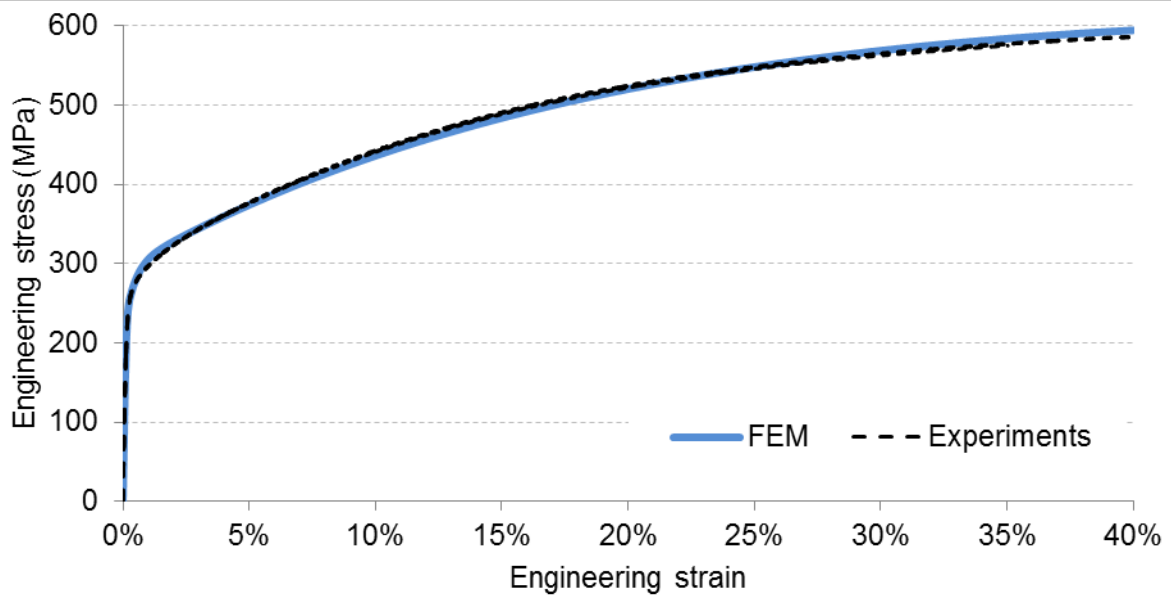


Figure 13. Verification of the material model in tension at constant strain rate $1 \cdot 10^{-5} \text{ s}^{-1}$

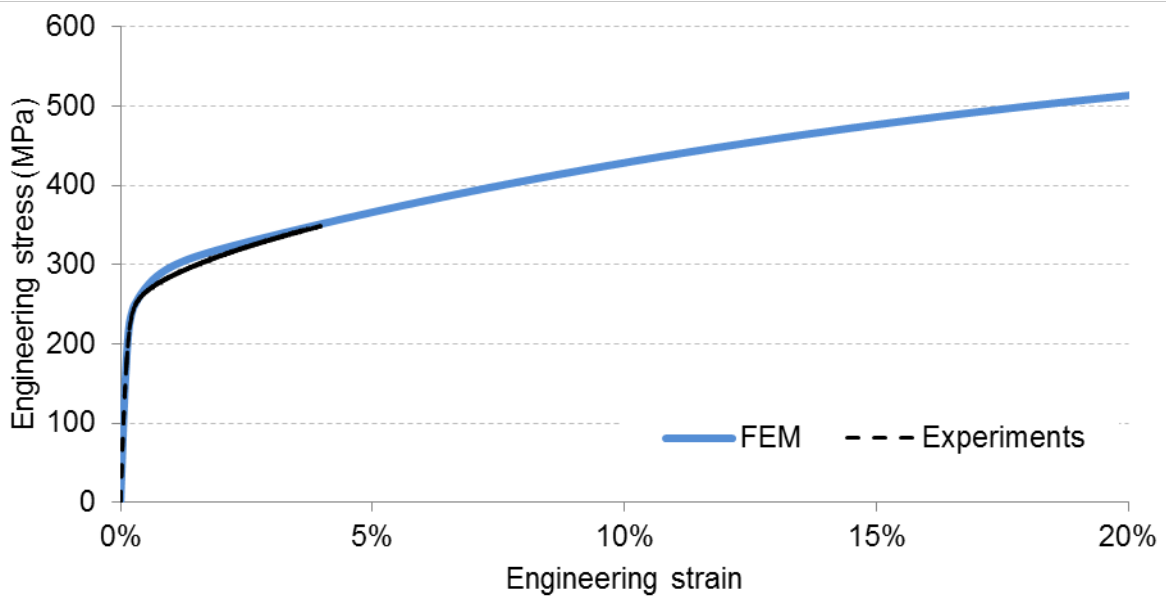


Figure 14. Verification of the material model in tension at constant strain rate $1 \cdot 10^{-6} \text{ s}^{-1}$

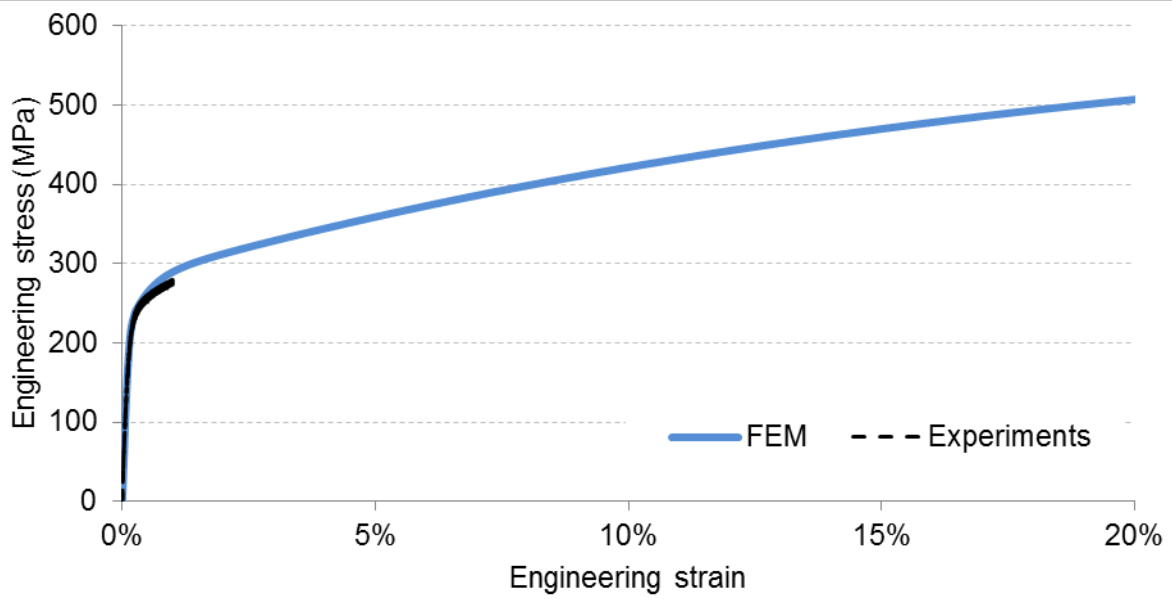


Figure 15. Verification of the material model in tension at constant strain rate $1 \cdot 10^{-7} \text{ s}^{-1}$

7.1.2 Validation of Chaboche model in creep

The same numerical models as described in the previous section were used to validate the material definition of austenitic steel plates in creep compared to the experiments from Task 5.1 of SIROCO project. The results are shown in Figure 16 to Figure 21.

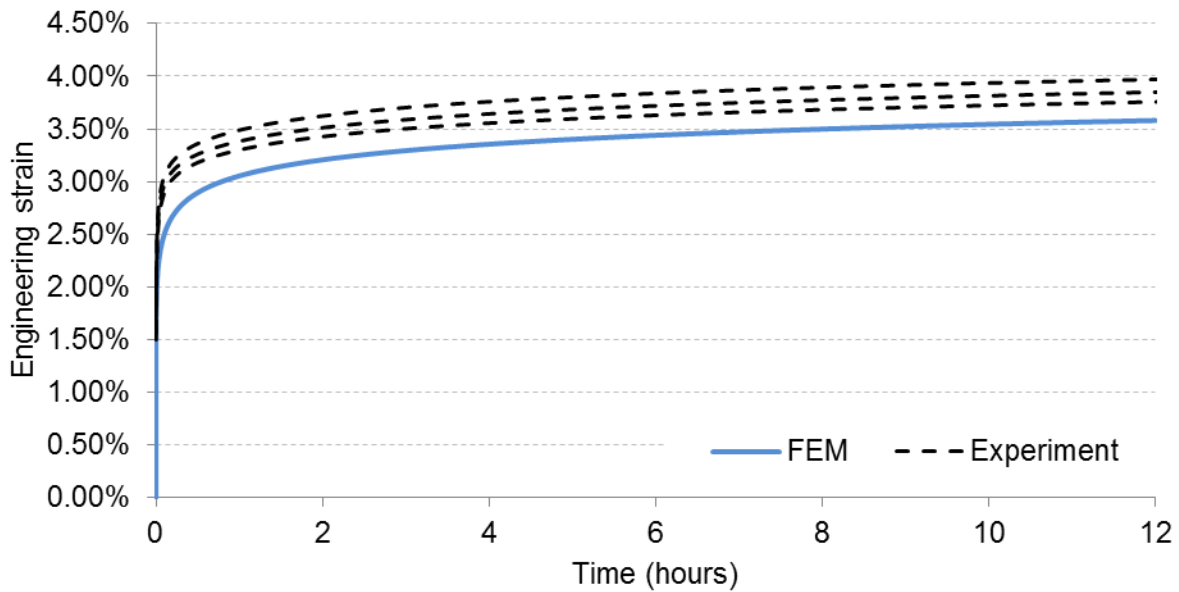


Figure 16. Verification of the material model behaviour at constant stress 336 MPa

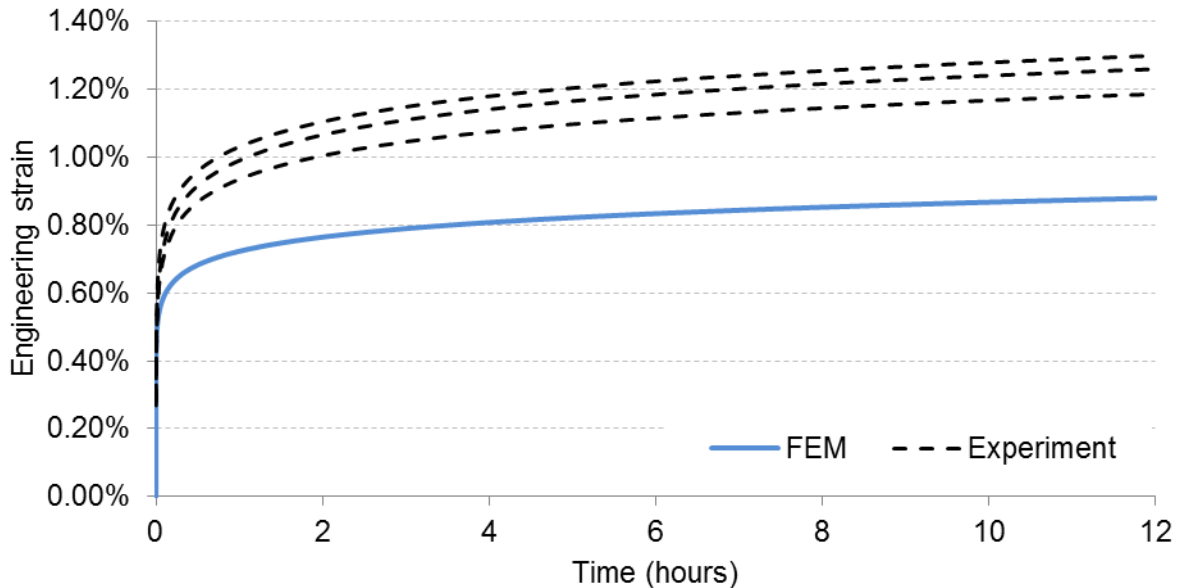


Figure 17. Verification of the material model behaviour at constant stress 280 MPa

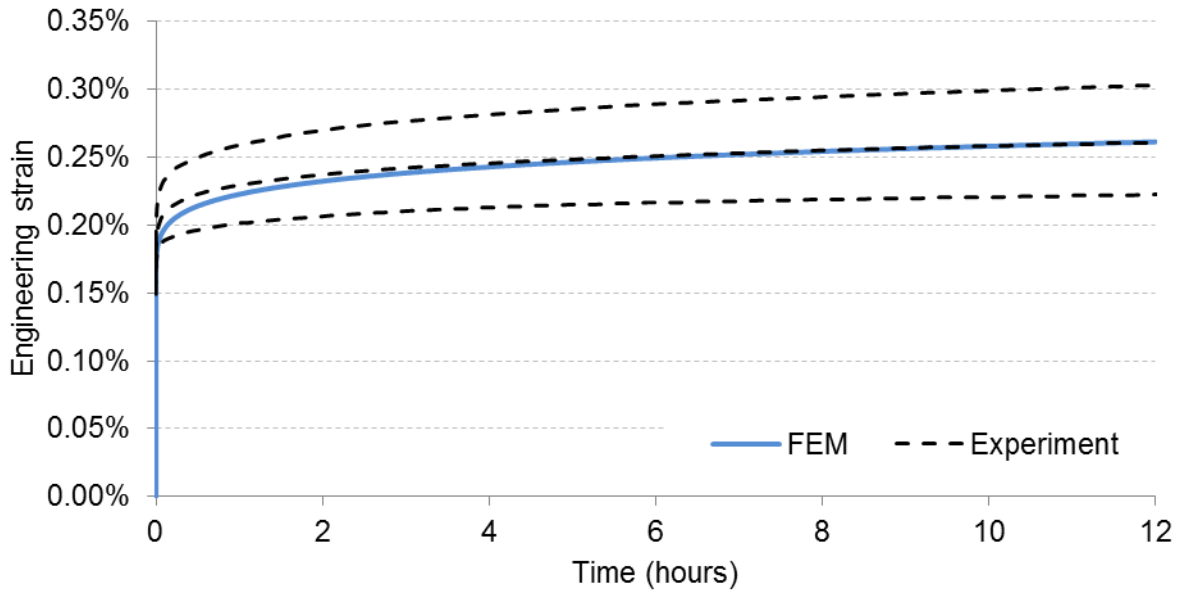


Figure 18. Verification of the material model behaviour at constant stress 231 MPa

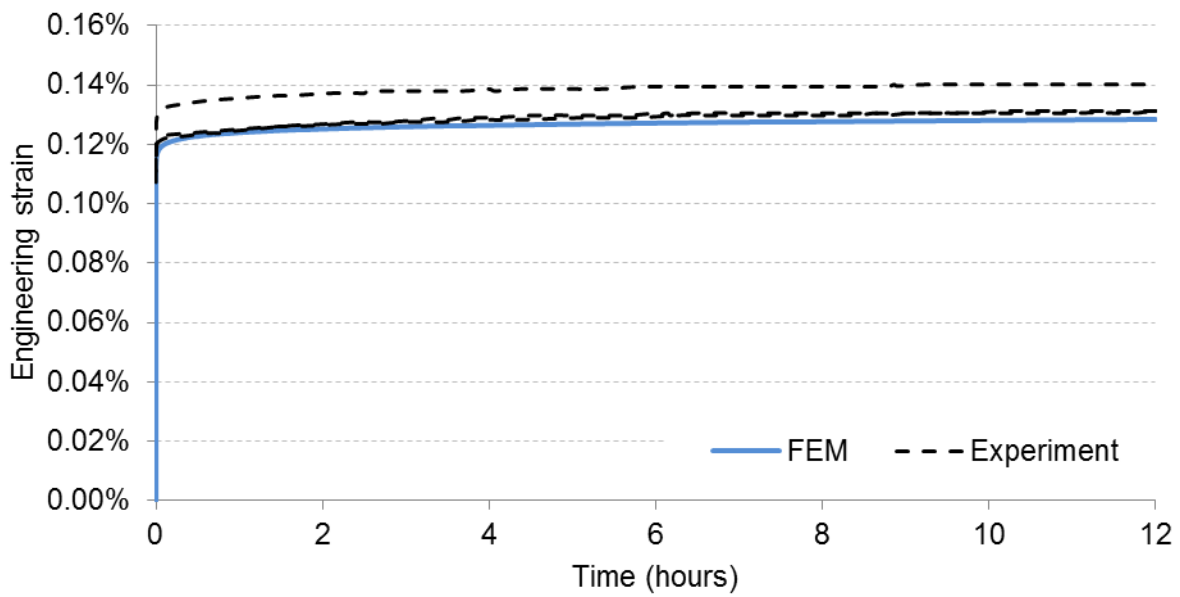


Figure 19. Verification of the material model behaviour at constant stress 182 MPa

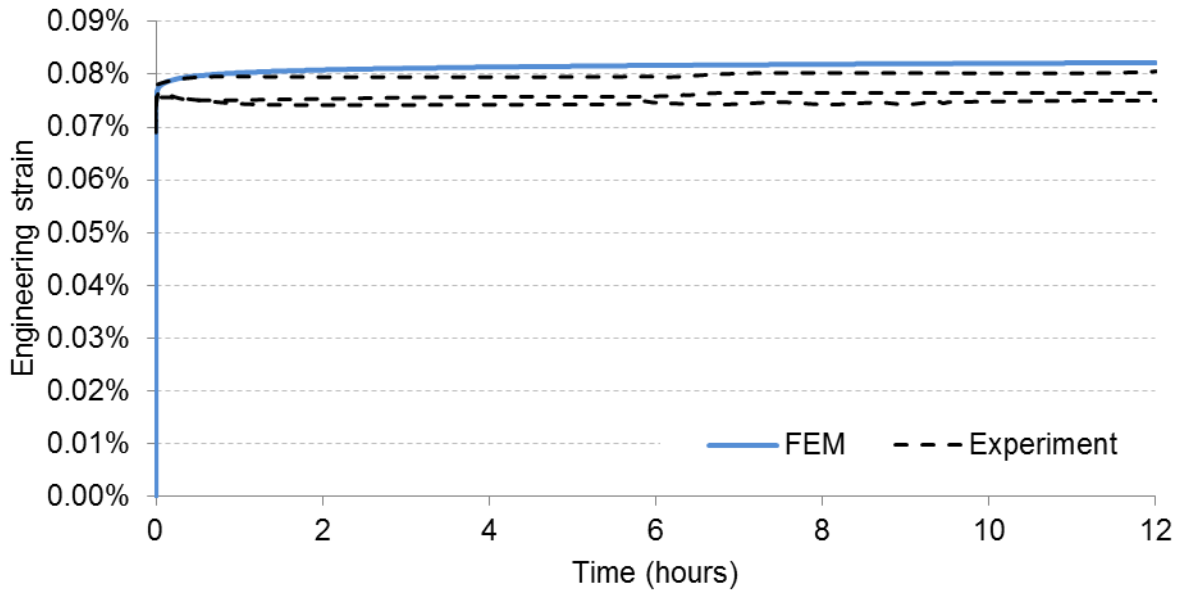


Figure 20. Verification of the material model behaviour at constant stress 133 MPa

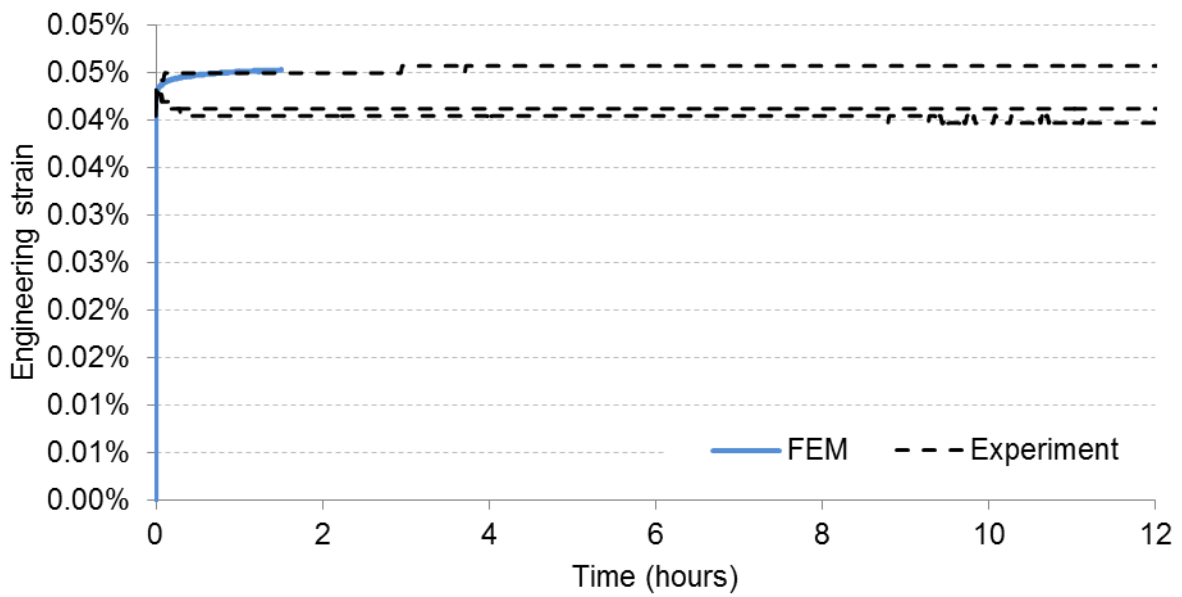


Figure 21. Verification of the material model behaviour at constant stress 84 MPa

7.1.3 Validation of Chaboche model in relaxation

The relaxation test of austenitic plates by VTT were not used for the model calibration, but their results showed very good match to the numerical prediction by the mixed isotropic and kinematic hardening model with strain rate dependent term as can be seen in Figure 22 to Figure 25. The recorded stress-strain behaviour during the pre-loading phase of the experiments served as an additional validation of the material non-linear behaviour in tension.

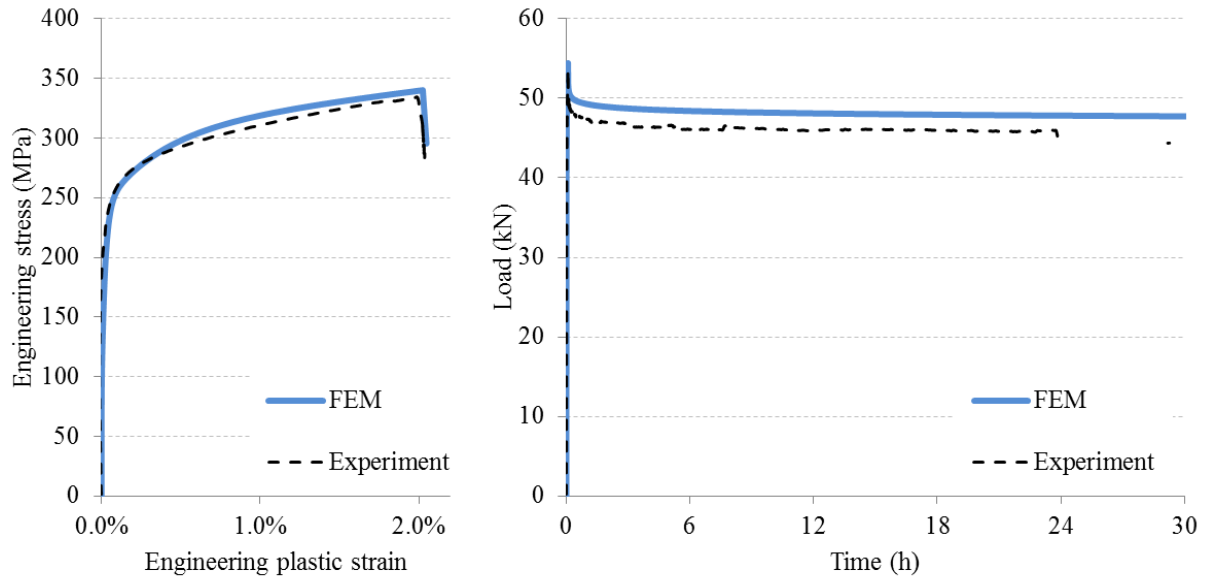


Figure 22 Verification of the material model behaviour at constant longitudinal strain 2.17% (right) and its pre-loading phase (left)

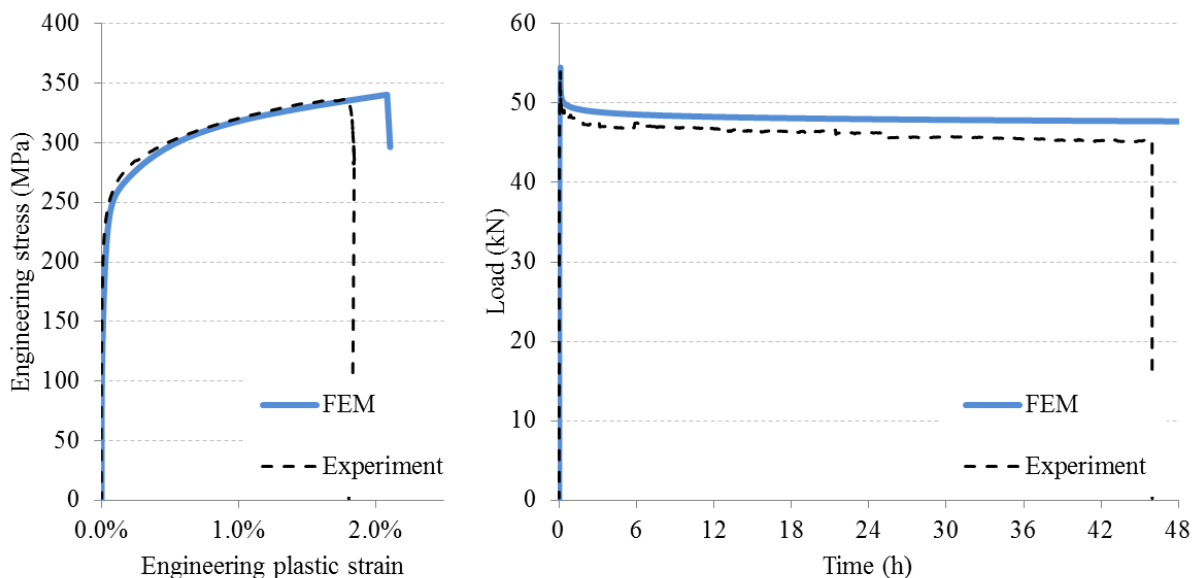


Figure 23 Verification of the material model behaviour at constant transverse strain 2.22% (right) and its pre-loading phase (left)

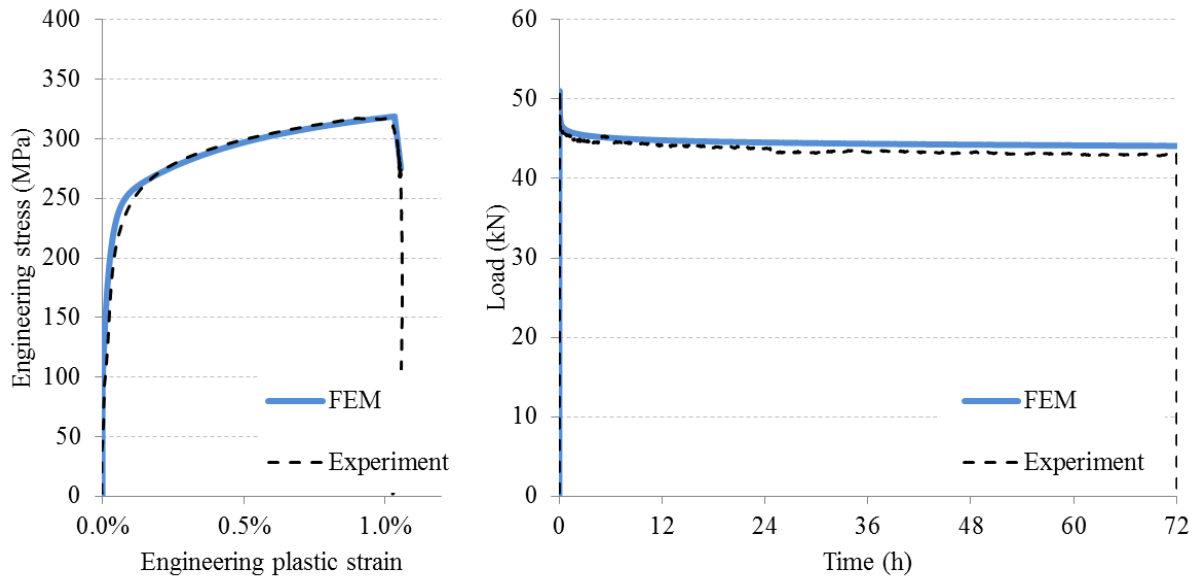


Figure 24 Verification of the material model behaviour at constant transverse strain 1.19% (right) and its pre-loading phase (left)

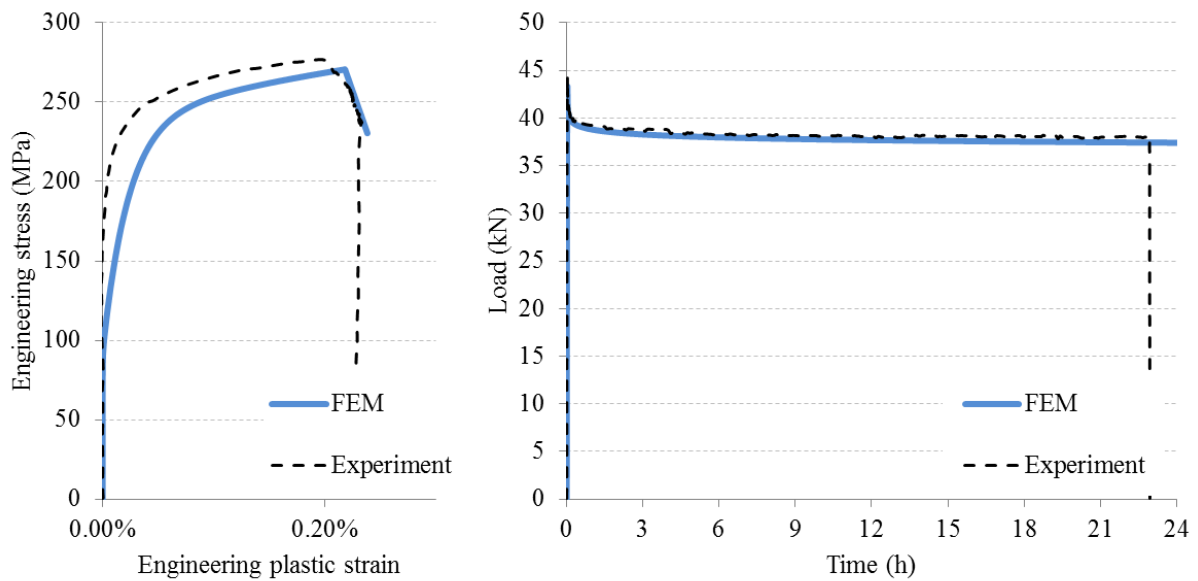


Figure 25 Verification of the material model behaviour at constant transverse strain 0.35% (right) and its pre-loading phase (left)

7.2 Material models for bolts

At load levels 60 % of R_{P02} and 100 % of R_{P02} the two parallel tests with LDX 2101 were nearly identical. At load level 80 % of R_{P02} the two test results differed from each other. The one in which the (t, σ) curve resembled the shape of same curve in the tests with different load levels was selected for fitting the model parameters (test y). The parameters of the models were fitted in Excel to three tests (preloading levels) simultaneously (tests x,y,z). The total stress drop in relaxation test at 60 % preload level was about 4.7 % of the preload, at 80 % preload level about 5.4 % and at 100 % preload level it was about 8.1 % of the preload.

7.2.1 Validation of time hardening model

The model was implemented into Abaqus as a CREEP subroutine. The time independent plastic behaviour was taken from true stress – true strain curves of tensile tests and implemented in Abaqus input file with the *PLASTIC option as shown in the example below:

```
*Material, name=Material-1
*Depvar
    6,
*Elastic
2.0d5, 3.5d-1
*Plastic
74.86000000,    0.0d0
74.86516391,    8.145d-07
75.33619216,    4.46249d-06
....
1016.215868,    0.06518043
1017.209332,    0.069041897
1017.937554,    0.075209096
```

The preloading rate was slightly different in the tensile tests and in the preloading of the relaxation tests, but the error caused but this in the modelled relaxation response was found to be small. It will be, however, possible to add preloading rate dependence into this model later.

Figure 26 shows the result of the relaxation model in Abaqus at 60% of R_{P02} preloading level compared with experiment. Figure 27 shows the result of the relaxation model in Abaqus at 80% of R_{P02} preloading level compared with experiment. Figure 28 shows the result of the relaxation model in Abaqus at 100% of R_{P02} preloading level compared with experiment.

316 CD 60 % RP02 relaxation

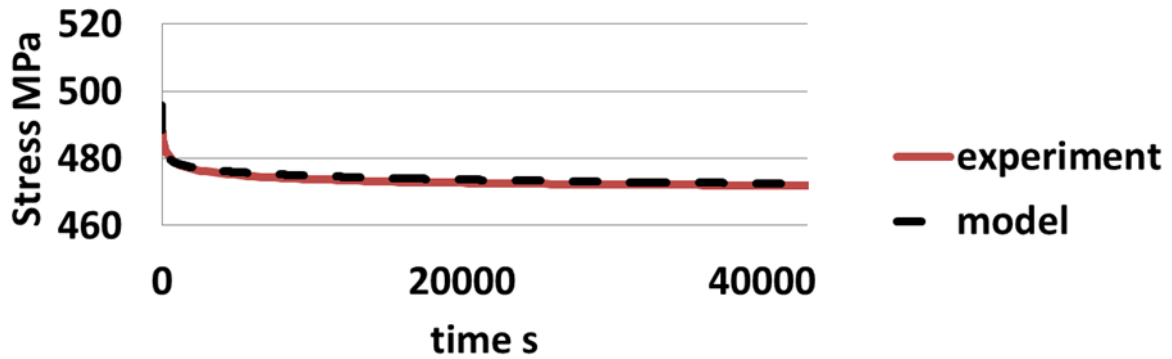


Figure 26 Time hardening relaxation model prediction at 60 % of R_{P02}

316 CD 80 % RP02 relaxation

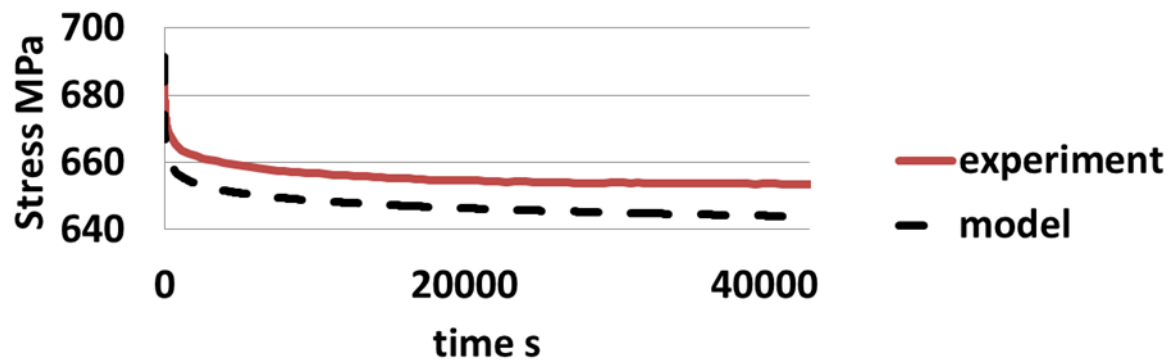


Figure 27 Time hardening relaxation model prediction at 80 % of R_{P02}

316 CD 100 % RP02 relaxation

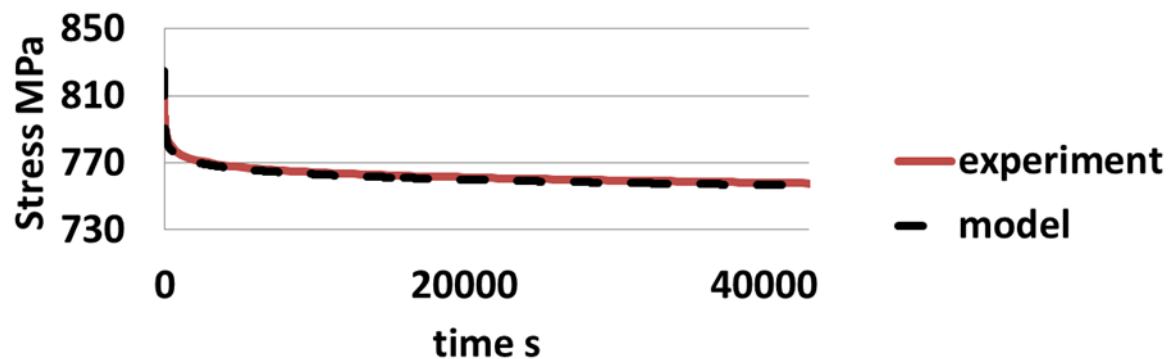


Figure 28 Time hardening relaxation model prediction at 100 % of R_{P02}

It can be seen that this time hardening type model predicts the relaxation behaviour with very good accuracy at high and low preload levels (less than 3% error in final stress compared to the total stress drop in experiment). At 80% of R_{P02} preload, the accuracy is not very good (about 26% error in final stress compared to the total stress drop in experiment).

It must be noted that this model is sensitive to time increments and especially the initial time increment. Currently the artificial elastic time in the beginning of relaxation (to avoid infinity near time zero) is made the same as the initial time increment. Too small initial time increment would give too large stress drop in the beginning. Too large time increment could give too large numerical errors. The recommended initial time increment is 0.1 s. The recommended maximum time increment is 8 s. Unfortunately, the initial stress drop behaviour is not the same in every test, and this is not properly represented with this time hardening model.

It must also be noted that the accuracy of the testing machine is not very good for this kind of experiment. Thus there may be relatively large errors (of order 0.5 %, which for example at initial load level 600 MPa is about 6-9 % of the total relaxation stress drop) in the stress measured.

7.2.2 Validation of strain hardening model

In addition, this model was implemented to Abaqus as a CREEP subroutine. This time the fitting was done utilising all the tests. Again the time independent plastic behaviour was taken from true stress – true strain curves of tensile tests and implemented in Abaqus input file with the *PLASTIC option. The nominal E modulus 200 GPa was used in separating the elastic and plastic strains as well for the elastic modulus in the ABAQUS model.

The preloading rate was somewhat different in the tensile tests and in the preloading of the relaxation tests, but the error caused by this in the modelled relaxation response was found to be small in the tests with cold drawn bars. It is possible to add preloading rate dependence into this model later.

Figure 29 shows the result of the relaxation model in Abaqus at 60% of R_{P02} preloading level compared with experiments for the austenitic 316 steel, using the parabolic and linear fit for the c parameter respectively.

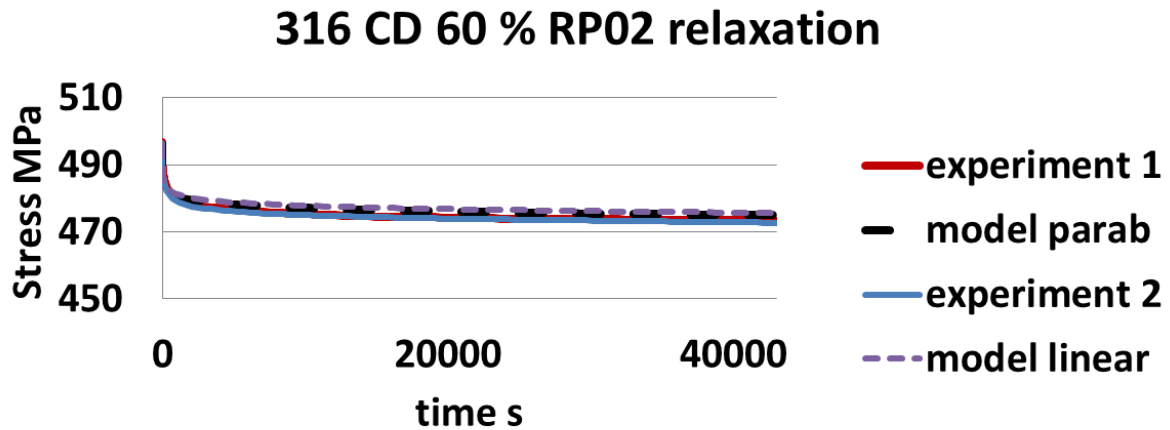


Figure 29 Strain hardening relaxation model prediction at 60 % of R_{P02}

Figure 30 shows the result of the relaxation model in Abaqus at 80% of RP02 preloading level compared with experiments for the austenitic 316 steel, using the parabolic and linear fit for the c parameter respectively.

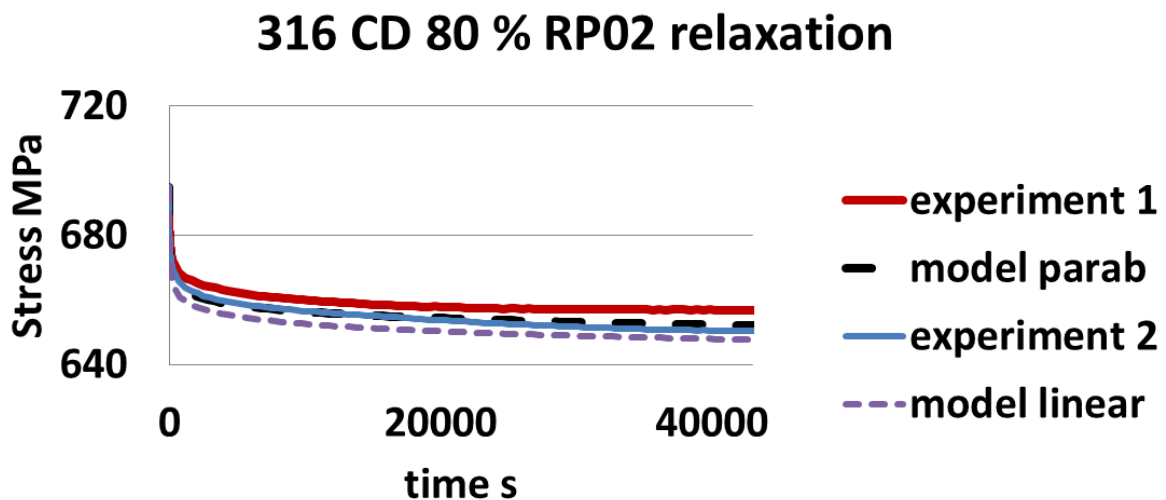


Figure 30 Strain hardening relaxation model prediction at 80 % of R_{P02}

Figure 31 shows the result of the relaxation model in Abaqus at 100% of RP02 preloading level compared with experiment for the austenitic 316 steel, using the parabolic and linear fit for the c parameter respectively.

316 CD 100 % RP02 relaxation

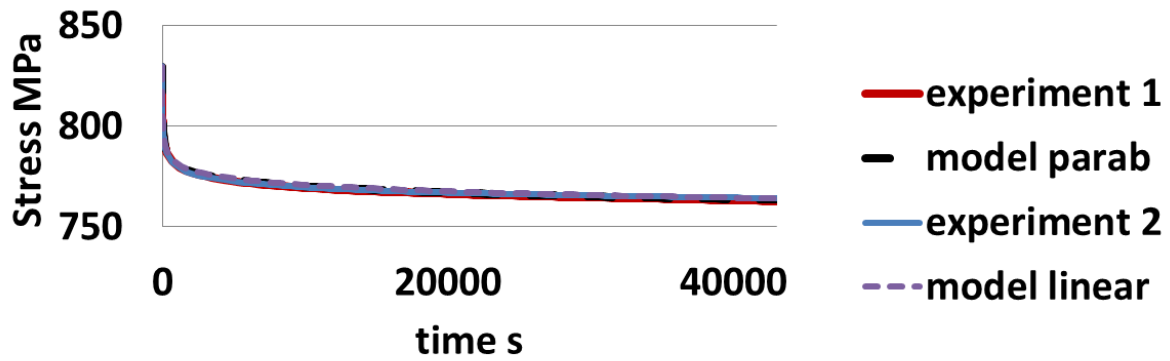


Figure 31 Strain hardening relaxation model prediction at 100 % of R_{P02}

It can be seen that this model predicts the relaxation behaviour with very good accuracy. Table 9 shows the errors between the modelled and experimental relaxation results for different cold drawn steels (18 results: two experiments per each of three load levels and three steel grades).

Table 9. Modelled stress drop compared to experiments with cold drawn steel bars

Grade	% of R_{p02}	error of parabolic fitting (MPa, %)		error of linear fitting (MPa, %)	
		MPa	%	MPa	%
EN 1.4401 (316) austenitic	60	1.3	5.9%	2.1	8.9%
		2.1	8.4%	2.7	11.5%
	80	-5.4	14.3%	-9.8	26.0%
		1.2	2.9%	-3.2	7.1%
	100	0.1	0.2%	0.7	1.0%
		-1.3	1.9%	-0.7	1.0%
EN 1.4162 (2101) lean duplex	60	1.8	7.2%	5.3	21.3%
		6.0	20.7%	9.5	32.7%
	80	7.5	16.4%	3.5	7.6%
		9.0	19.0%	5.0	10.6%
	100	11.0	14.2%	10.3	13.2%
		10.4	13.6%	9.7	12.6%
EN 1.4462 (2205) duplex	60	1.7	6.6%	1.5	5.9%
		1.2	4.8%	1.0	4.0%
	80	-0.5	1.0%	-5.6	11.0%
		-2.8	5.8%	-8.0	16.2%
	100	-6.8	7.4%	-0.4	0.5%
		-12.2	14.2%	-5.8	6.8%
Average		1.4	9.1%	1.0	11.0
Maximum			20.7%		32.7%

Thus, the accuracy of the model was in average good (less than 15 % error) with the cold drawn bar tests of austenitic 316 steel, stainless 2205 steel and LDX 2101 steel. The maximum error was with LDX2101 steel at 60 % of R_{p02} using linear fit for the c parameters (32.7 % and 21.3 % of the total stress drop) and with 316 austenitic steel at 80% of R_{p02} using linear fit for the c parameters (26 % and 7.1 % of the total stress drop). With LDX at higher initial stresses the accuracy was much better, and with 316 at the lower and higher initial stresses the accuracy was much better. In the tensile test of 316 cold drawn bar, there was a 10 MPa artificial stress in the beginning of the tensile test. This could affect the results, because at that stress level the total stress drop in the relaxation test was only about 23 MPa. With LDX, the two relaxation tests at 80 % of R_{p02} gave significantly different results. The parabolic fit for c parameters gave somewhat better results than the linear fit. A larger set of experiments in the fitting might improve the accuracy of the model.

This model is not very sensitive to time increments. The recommended initial time increment for the relaxation step in ABAQUS is 0.2 s. The recommended maximum time increment is 500s.

This strain-hardening model is recommended for modelling relaxation in steel bolts, especially when multiple bolts are loaded in sequence or retightening is used. An important future development could be adding the effect of the preloading strain rate, but that would need more experiments.

The model was considered also for modelling relaxation tests with bars machined from rebar of 316 and 2101 steels, and a year later also for 2205 annealed steel bar.

The shape of the relaxation curve was very similar in all tests, and as an analytical model this model works well for all the relaxation tests. Unfortunately, the stress strain curves of the tensile part of the 2205 annealed bar relaxation test and the corresponding tensile test were very different. There was also some difference in the tensile part of relaxation test of LDX 2101 and the corresponding tensile test. Thus, the ABAQUS model utilising tensile test results for the time independent plasticity works well only with the tests with cold drawn bars of as received material. The stress-strain curves in the tests with rebar materials and annealed bar of 2205 were also rather different from the tensile tests of the as received cold drawn material. The difference is probably due to the machining of the rebar material, and for the 2205 annealed bar due to the annealing and due to the previous creep tests.

The ABAQUS model uses the stress - plastic strain relationship from the tensile tests for the time independent plasticity. The nominal E modulus was used in the model for all tests. In the tests, the E modulus of 316 cold drawn steel was very low, but that was probably due to the fact, that these bars were not straightened before the test, so there was some bending as well. Thus, the nominal value 200 GPa was used also for this material.

In the future, the model should always be used with the tensile part of the relaxation test for the time independent plasticity, instead of results of a separate tensile test. This emphasises the fact that the preloading actually has a relatively large effect on the relaxation behaviour. Especially the difference shows in the fast relaxation in the beginning of the relaxation test.

It must be emphasised that this model is not enough for rigorous representation of the relaxation behaviour of steels. Adding the effect of the strain rate of the tensile part of the relaxation test into the model would improve the results. An alternative is a more physical model that takes into account all hardening related aspects. An empirical model can only be a crude approximation as the steel material evolves so much in each treatment. As there are different manufacturing methods for steel bolts and that include machining, a more rigorous model will be needed in the future. Anyhow, this model serves as a simple and easy to use approximate model for relaxation of steel bolts. The time independent plasticity could also be represented by some function in order to further ease the use of the model.

In the future it would be important to make more tests using different preloading rates, and also tests with retightening. By adding the dependency on preloading rate and modelling experiments with retightening, it would be possible to predict the loss of the tightening force in bolt assemblies and schedule the pre-tightening optimally.

8. Connection behaviour

8.1 The effect of model geometry

Eight different models were calculated with the same material parameters and their loss of preload after 50 years was compared in order to verify the effect of (a) model dimensionality, (b) horizontal symmetry (bolt head is assumed to behave the same way as the nut) and (c) relaxation of thread in the nut. They are presented in Figure 33 and Figure 34.

The Table 10 shows the preload needed to achieve 70% f_y in the bolt shank, its loss after 50 years and the calculation time on Quad-Core AMD Opteron(tm) Processor 2354 with 32 GB RAM. The loss of preload is also demonstrated in Figure 32.

Table 10 The effect of model geometry

Dimensionality	Threads	Symmetry	Preload	Loss of preloading force after 50 years	Calculation time
2D axisymmetric	No	No	117 kN	17.7%	8 min
		Yes	123 kN	17.7%	6 min
	Yes	No	113 kN	17.4%	10 min
		Yes	117 kN	17.4%	8 min
3D symmetric in two vertical planes	No	No	135 kN	17.8%	8 h 5 min
		Yes	135 kN	18.0%	2 h 10 min
	Yes	No	131 kN	17.7%	19 h 56 min
		Yes	130 kN	17.8%	2 h 44 min

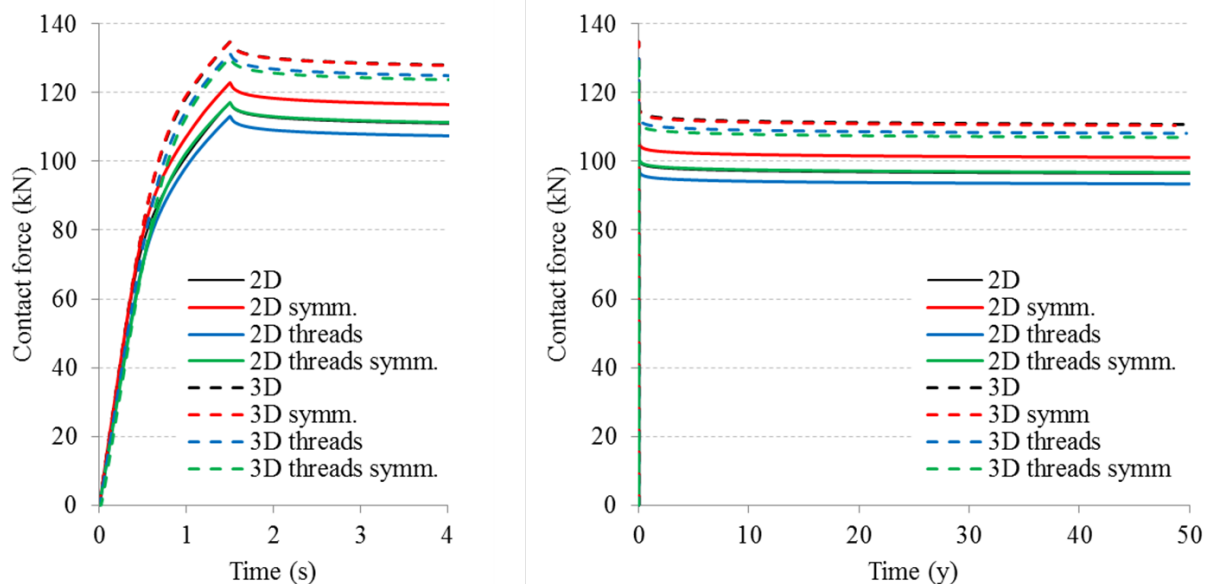


Figure 32 Loss of contact (preload) force during the time

It is clear that the 2D models provide more conservative results than 3D models, but also the use of threads results in greater preload loss during pre-tightening. Therefore, it is recommended that threads are included in the future studies even if their calculation is more computationally expensive.

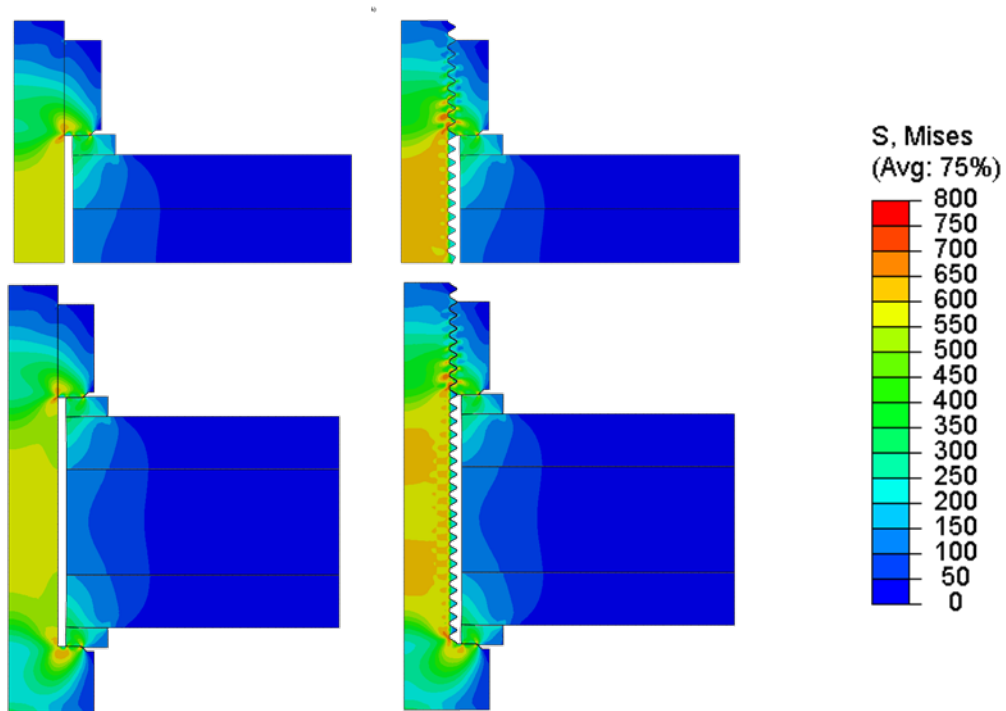


Figure 33 2D axisymmetric models used in the study

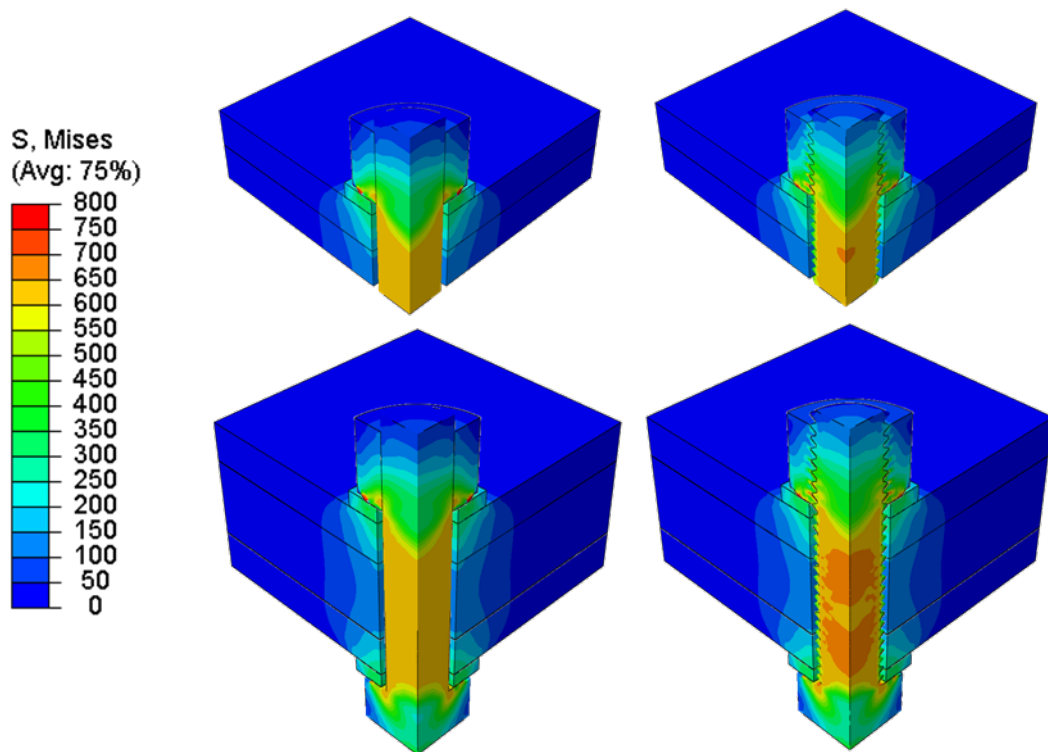


Figure 34 3D models used in the study

8.2 The effect of preloading rate

The different pre-loading rates were studied using the 2D axisymmetric models of M12 bolt assembly described in Figure 35.

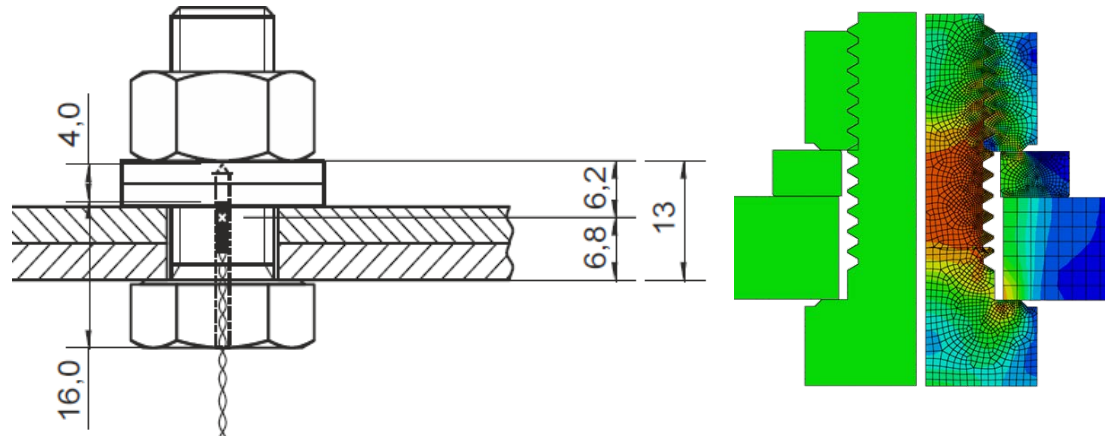


Figure 35 Drawing of the assembly (left) and the FE model (right)

The rates were ranging from 10 RPM to 0.1 RPM resulting in the pre-tightening time from 1 s to 189 s and bolt head rotation from 57 to 113 degrees due to the different relaxation in pre-loading phase. The differences in the preload loss were significant after 90 hours and were not decreasing (see Figure 36). Therefore, we concluded that the preloading speed is an important parameter for the stainless steel bolts execution and the lower speed results in lower preload loss due to the relaxation.

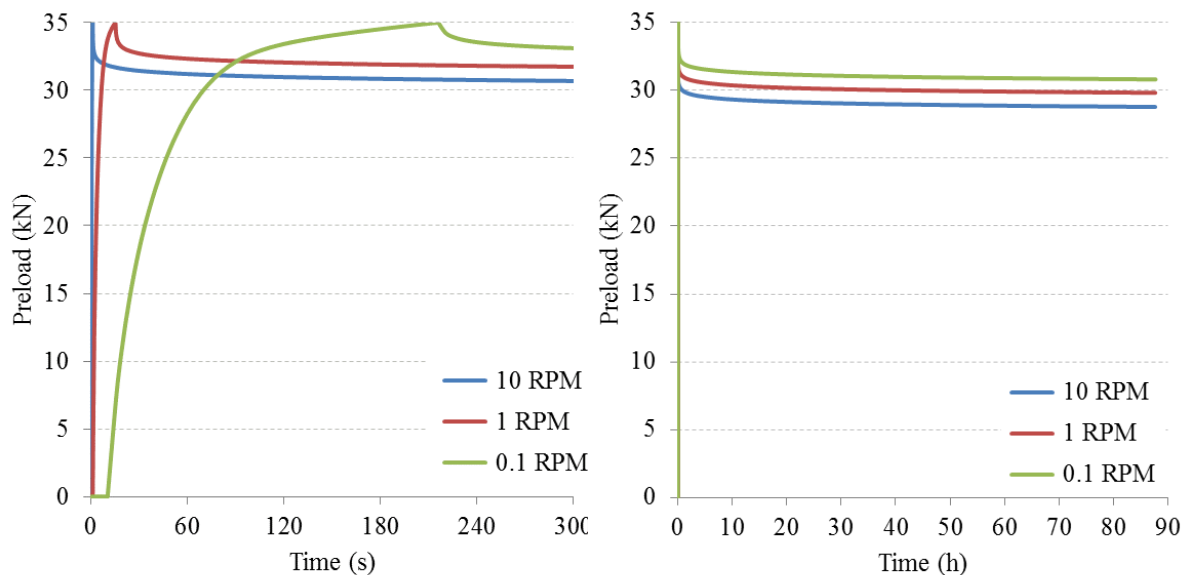


Figure 36 Loss of the preload after 300 seconds (left) and 90 hours (right)

8.3 The effect of re-tightening

The use of UAMP subroutine to control the pre-loading force enabled us to examine the effect of re-tightening of the bolts after a certain period. We have simulated the assembly with M16 bolt, nut and washer (ISO 4017, EN ISO 4032, EN ISO 7091) loaded to 70% of f_y (630 MPa)

Plates 8 mm + 16 mm + 8 mm) and 2D axisymmetric model preloaded to reach 70% of yield strength in the shank (630 MPa). It should be noted that the maximum von Mises stress in the model was 104% of the yield strength in the thread (see Figure 37).

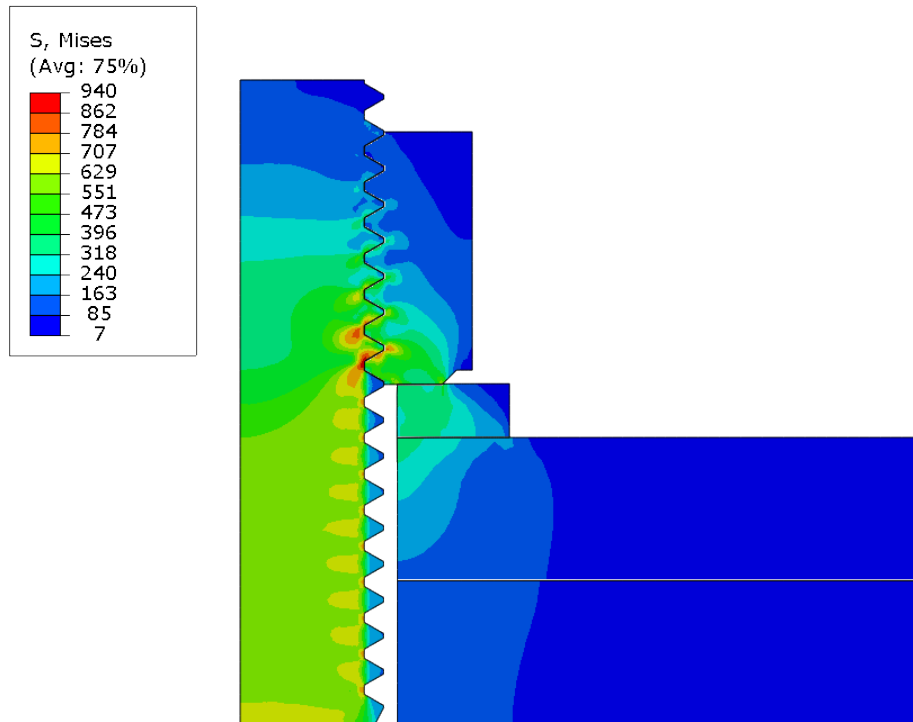


Figure 37 Von Mises stress distribution in the model

Three cases were considered

- (a) Single preloading at 10 RPM without any re-tightening and relaxation 50 years
- (b) Re-tightening after 5 years and relaxation 45 years
- (c) Re-tightening after 5 and 10 years and relaxation 40 years.

Their results are compared in Figure 38. It shows that the re-tightening is significantly improving the bolt performance, but the effect is gradually lower.

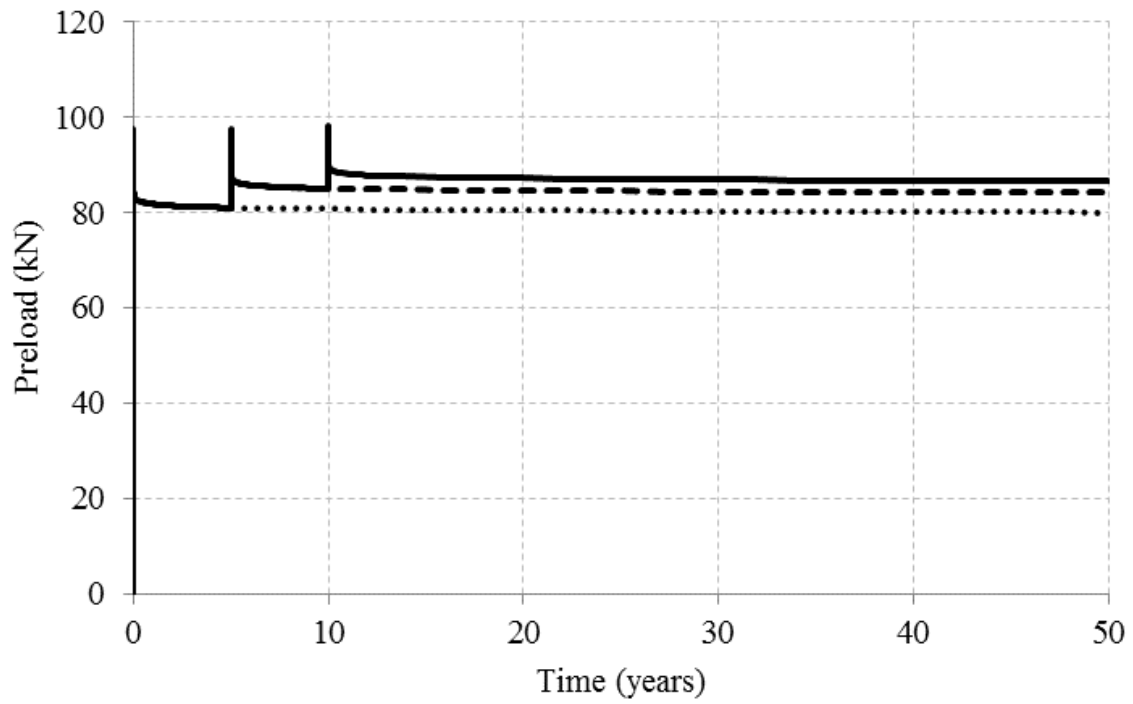


Figure 38 The loss of the preload (contact force) in models without re-tightening (dotted line) and models with re-tightening after 5 years (dashed line) and 5 and 10 years (solid line)

8.4 Slip behaviour

The objectives of the work presented in this section are to (i) develop in Abaqus a numerical model of the slip factor test according to EN1090-2 [27], (ii) examine the role of the static coefficient of friction in the behaviour of the slip test and (iii) calibrate the numerical model against available University of Duisburg-Essen (UDE) and Technical University in Delft (TUD) test results of carbon steel.

In the subsequent work in Task 6.4 the current FE model (based on carbon steel) will be extended to include a stainless steel material model to simulate the stress relaxation/creep in slip resistant joints made of various grades of stainless steel. The extended model will be further calibrated against UDE and TUD test results of stainless steel slip tests.

8.4.1 Introduction

A series of slip factor tests using carbon steel were carried out at UDE and TUD. Tests were undertaken at three different clamping lengths: 152, 83 and 52 mm. The experimental set-up and corresponding FE models are shown in Figure 39.

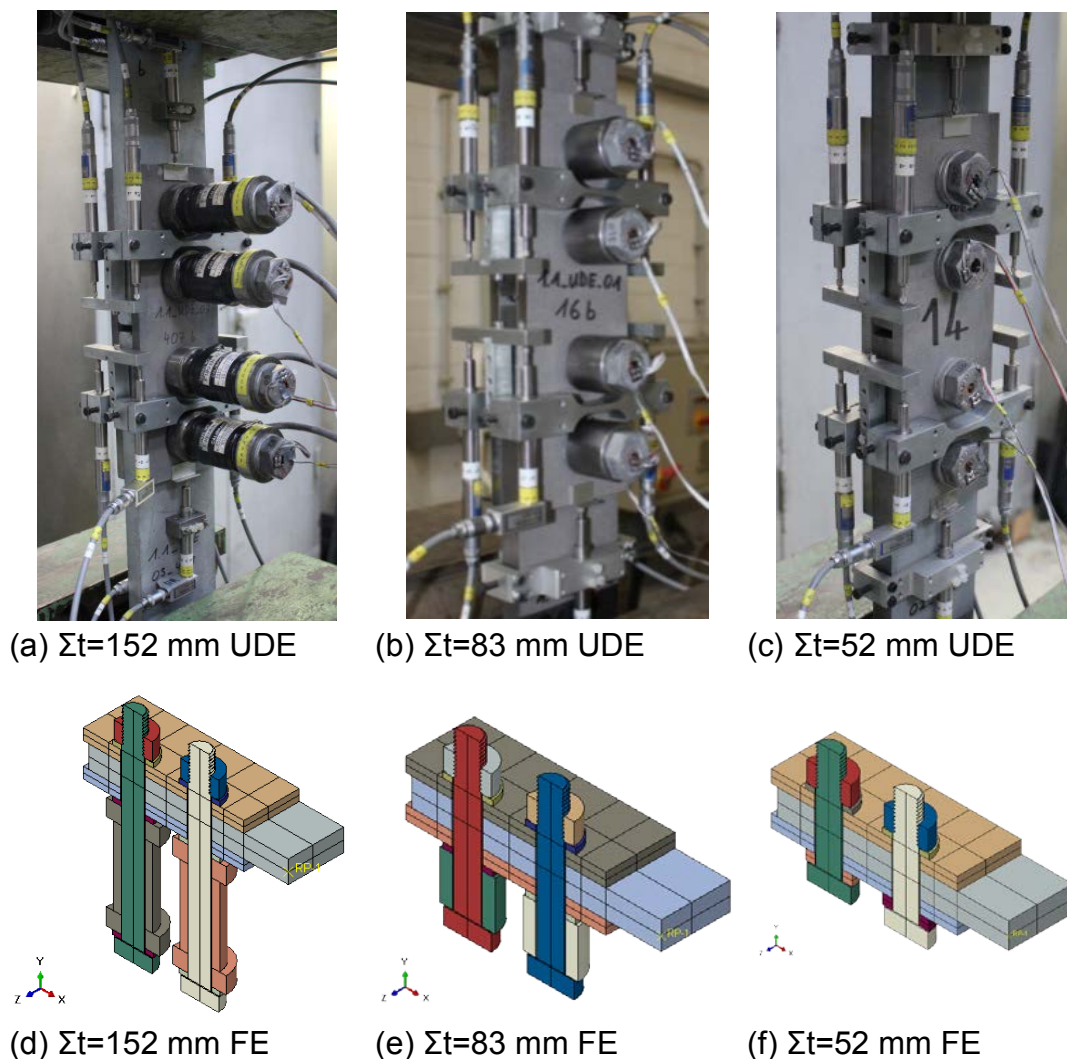


Figure 39 Slip test and Abaqus FE model of different clamping length

The carbon steel of the plate was S355J2C+N. M20 HV 10.9 carbon steel bolts were used in the slip test. The plate surface was grit blasted (GB) with reported static coefficient of friction (μ_{fric}) of 0.48 – 0.55.

Elastic – perfectly plastic material models were used for all parts of the test connection. The elastic modulus and yield stress are shown in Table 3. The material used for the extension adaptors was assumed to be the same as the plates.

Table 11 Material properties of each component of the test connection

	Bolt	Nut	Plate/Adaptors	Washer
σ_y	918 MPa	1020 MPa	362.1 MPa	979.2 MPa
E	210 GPa			

No retightening was modelled in the FE model at this stage. The preload was applied using Abaqus load type “bolt load” to the level of 172 kN for M20 10.9 bolts.

8.4.2 Static coefficient of friction

In a slip resistant connection, the shear load is resisted by the friction between the faying surfaces of the clamped plates. The static coefficient of friction plays an important role in the prediction of the individual slip load and the slip factors as well. In the numerical model, the Coulomb friction model is used. The shear stress (τ) is related to the normal pressure (p) by the coefficient of friction (μ_{fric}) as $\tau = \mu p$.

The static coefficient of friction between grit blasted carbon steel surfaces was reported to be 0.48 – 0.55 (Section 8.4.1). A pre-study was carried out to determine the influence of μ_{fric} on the slip response of the FE model. A model with clamping length of 52 mm was used in the pre-study and μ_{fric} was varied between 0.5 – 0.9. The results are presented in Figure 40 and compared with UDE test results (GB-III in Figure 40). The coefficients of friction for all other contact surfaces (bolt – washer, plate – washer etc.) were assumed to be 0.5 for simplicity and consistency.

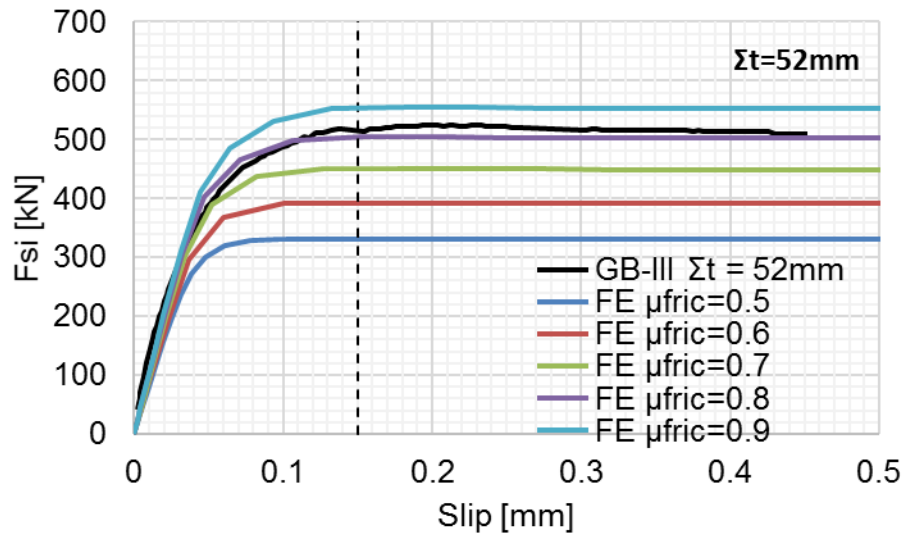


Figure 40 Effect of static coefficient of friction on the shear load slip displacement curves ($\Sigma t = 52$ mm)

It is evident from Figure 40 that the slip load F_{si} at a slip displacement of 0.15 mm increased when μ_{fric} was increasing from 0.5 to 0.9. The initial and actual slip factors at different values of μ_{fric} were calculated and presented in Table 12. The actual bolt clamping force $F_{p,C,act}$ and coefficient μ_{actual} at slip of 0.15 mm are also shown.

Table 12 Individual slip load and slip factors for different coefficient of friction ($\Sigma t = 52$ mm)

μ_{fric}	F_{si} (kN)	$F_{p,C,act}$ (kN)		μ_{ini}	μ_{actual}
		bolt A	bolt B		
0.5	330.5	164.2	166.7	0.480	0.499
0.6	391.8	162.0	165.6	0.569	0.598
0.7	449.8	159.4	163.9	0.653	0.696
0.8	503.8	156.2	161.6	0.731	0.793
0.9	553.3	152.6	158.9	0.802	0.888

Figure 41(a) shows that the slip load F_{si} increased and bolt preload $F_{p,C}$, decreased when μ_{fric} was increasing. Figure 41(b) shows that both initial and actual slip factors increased when the friction coefficient μ_{fric} was increasing. It can be noted that the actual slip factors is increased by a greater amount than the initial factor, because of the higher loss of preload occurred at larger μ_{fric} .

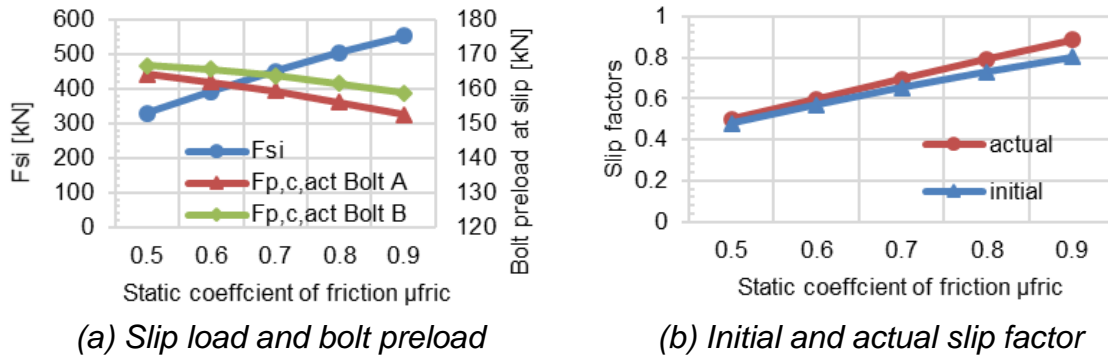


Figure 41 Influence of the static coefficient of friction on the slip load, preload and slip factors ($\Sigma t=52$ mm, M20 HV 10.9)

8.4.3 Preliminary validation of FE models (carbon steel)

It can be observed in Figure 40 that the numerical slip load – displacement was in reasonably good agreement when μ_{fric} was assumed to be 0.8. In this preliminary validation work, the value of the friction coefficient μ_{fric} was determined so that the initial slip factor μ_{ini} is exactly the same as measured in the UDE test with a clamping length of 52 mm (Series ID: GB-III).

It was found that by assuming the friction coefficient μ_{fric} equals to 0.817 in the FE model, the initial slip factor (for $\Sigma t = 52$ mm) was determined to be $\mu_{ini} = 0.744$ which is almost the same as the test (0.74). The numerical slip load – displacement curve with $\mu_{fric} = 0.817$ is compared with the test results of GB-III test in Figure 42, Figure 43 and Figure 44 where favourable agreement is obtained at central point and edge (CBG and PE in the graphs).

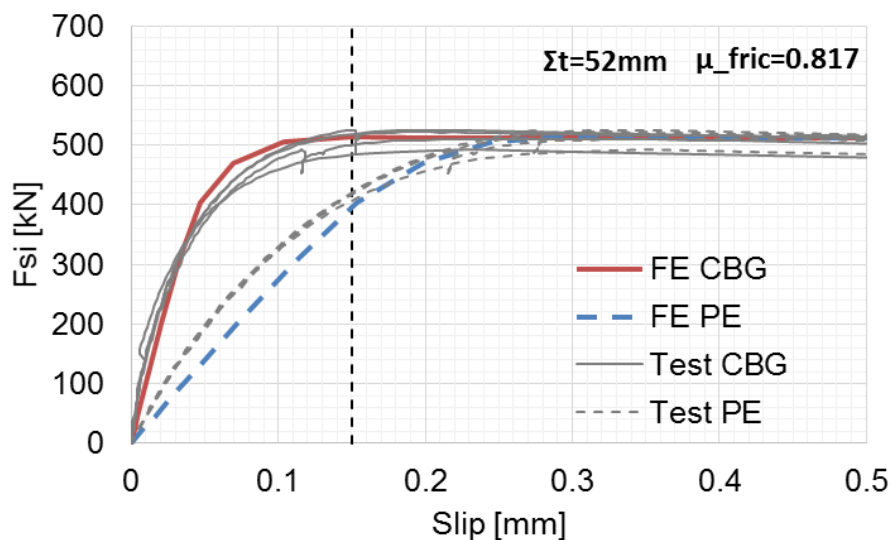


Figure 42 Comparison of slip load – displacement curve predicted using Abaqus with UDE test ($\Sigma t = 52$ mm and $\mu_{fric} = 0.817$ for Abaqus)

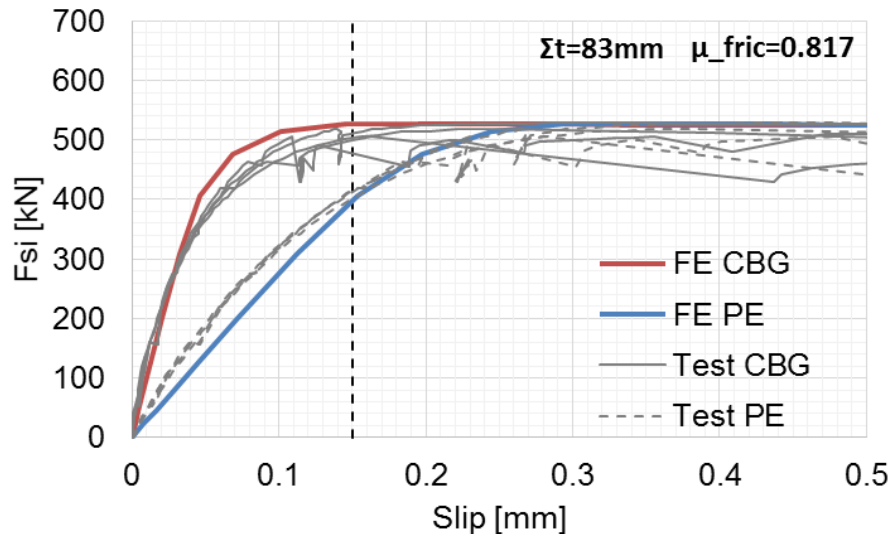


Figure 43 Comparison of slip load – displacement curve predicted using Abaqus with UDE test ($\Sigma t = 83 \text{ mm}$ and $\mu_{fric} = 0.817$ for Abaqus)

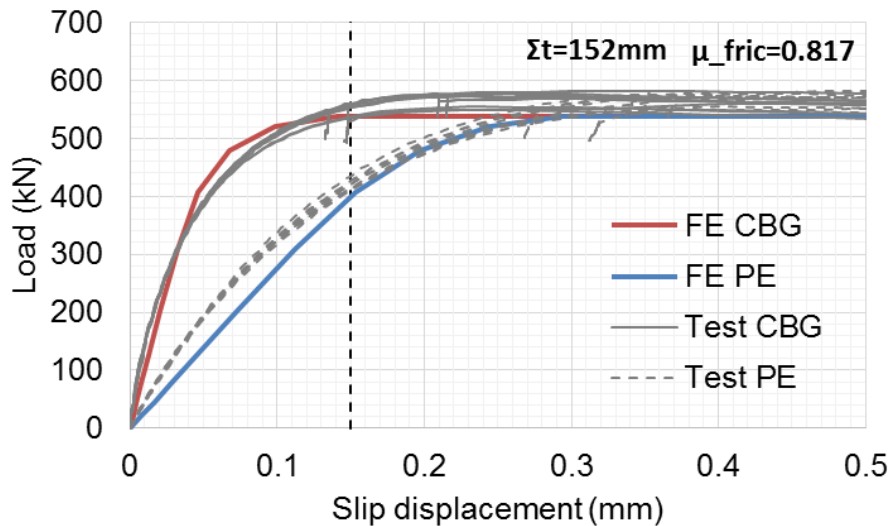


Figure 44 Comparison of slip load – displacement curve predicted using Abaqus with UDE test ($\Sigma t = 152 \text{ mm}$ and $\mu_{fric} = 0.817$ for Abaqus)

The static coefficient of friction $\mu_{fric} = 0.817$ was therefore used for all subsequent numerical analysis for a grit blasted carbon steel surface. This ensures consistency when comparing with other test data and allows examination of the accuracy/validity of the assumed value of $\mu_{fric} = 0.817$ for grit blasted surface of carbon steel in general.

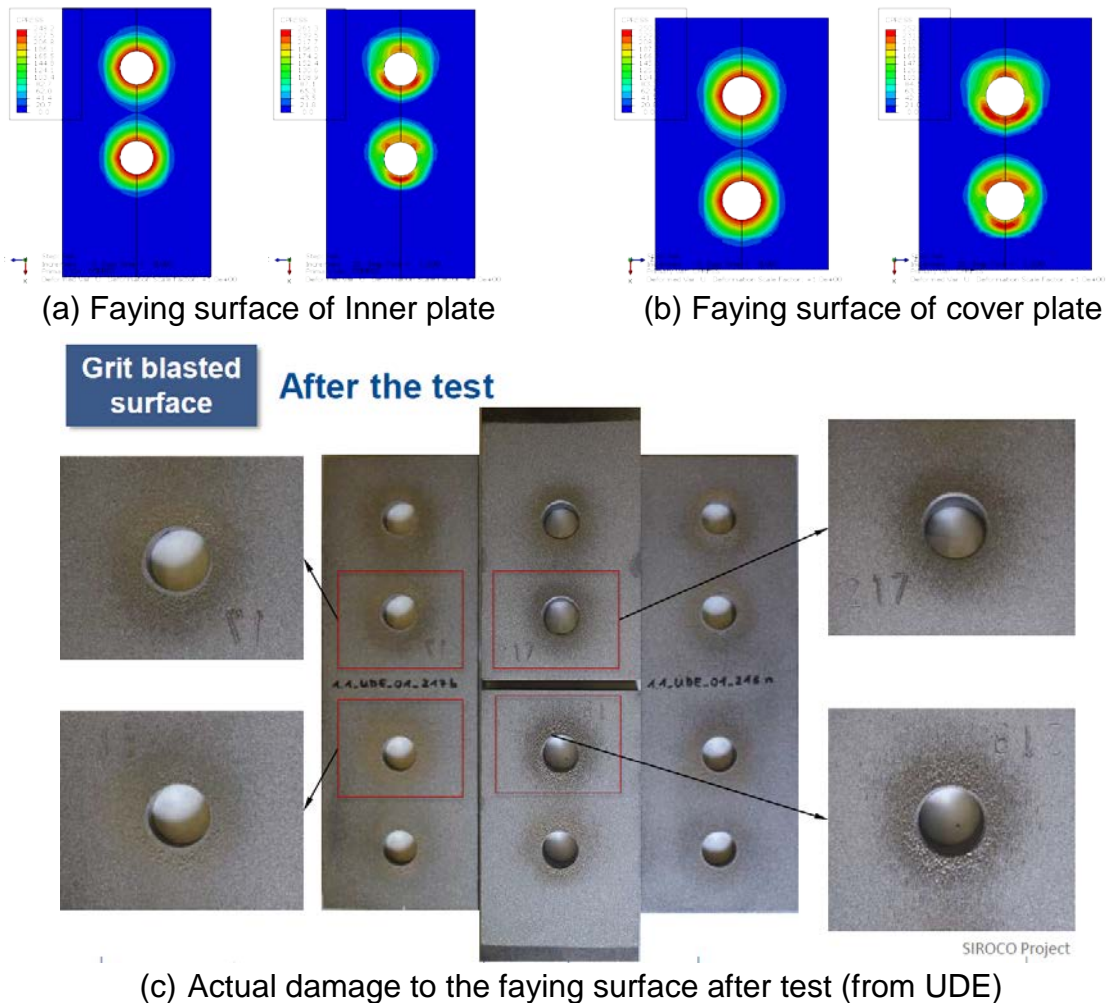


Figure 45 (a) & (b) – pressure distribution over the faying surface between cover plate A and inner plate (left: under preload, right: after slip test); (c) – actual damage of the faying surface after test

Figure 45 compares the high contact pressure areas in the FE model with the actual observation made after the test. Figure 45(a) shows the contact pressure before and after the slip test over the faying surface of the inner plate. Figure 45(b) shows the contact pressure over the faying surface of the cover plate. The area of the FE model under high contact pressure is very similar to the area of surface damage due to high compressive pressure found in the test.

The surface damage observed after testing suggested that the high spots on these roughened surfaces are likely to be yielding in compression. It is possible that, at these pressures, friction is not independent of normal contact pressure. This might explain the coefficient of friction used in the numerical model ($\mu_{fric} = 0.817$) is greater than the reported value between 0.48 – 0.55.

Additional numerical studies were carried out at longer clamping lengths but all assuming $\mu_{fric} = 0.817$. All available slip factors predicted by FE model are compared with UDE and TUD test results in Table 4 below. Over the three clamping lengths, the difference between the predicted slip factors assuming $\mu_{fric} = 0.817$ and the measured values are within 10%. Two values of actual bolt load ($F_{p,c,actual}$) are for bolt A and B measured at the slip displacement of 0.15 mm.

Table 13 Comparison of numerical slip factors at CBG with tests ($\mu_{fric} = 0.817$)

Σt		F_{si} (kN)	$F_{p,c,actual}$ (kN)		μ_{ini}	μ_{act}
52 mm	UDE	505.5	147.3		0.74	0.86
	TUD*	-	-		0.67	0.81
	Abaqus	513.4	155.6	161.2	0.744 (0.5% ¹ ; 11% ²)	0.810 (-5.8%; 0%)
83 mm	UDE	474.65	153.9		0.70	0.78
	TUD	-	-		-	-
	Abaqus	526.3	160.9	164.0	0.766 (3.5%; -)	0.810 (-2.4%; -)
152 mm	UDE	549.1	171.8		0.80	0.87
	TUD**	-	-		0.79	0.85
	Abaqus	536.9	164.7	166.9	0.78 (-2.5%; -1.3%)	0.810 (-6.8%; -4.7%)

M20, HV10.9; S355 plates, $\mu_{fric} = 0.817$ for grit blasted surface of carbon steel in Abaqus, slip measured at CBG

* $\Sigma t = 48$ mm, 10 min slip test time

** 24 min slip test time

1 % difference between UDE measured and predicted value

2 % difference between TUD measured and predicted value

It should be noted that TUD had not carried out a test with a clamping length of 83 mm and the shortest clamping length was actually 48 mm, although their results are compared with a clamping length of 52 mm from UDE and FE. The slip test time was 24 minutes for the test with a clamping length of 152 mm, which is slightly longer than UDE's 15 minutes. The FE model for carbon steel does not consider any time dependent behaviour.

Figure 46 compares graphically the initial slip factor between numerical model (Abaqus), UDE and TUD at three different clamping lengths: 52, 83 and 152 mm. It can be seen that the initial slip factors are well predicted by the numerical model at all three clamping lengths. The numerical model also correctly reproduces the influence of the clamping length on the slip factors. The initial slip factors increase when the clamping length is increased due to a reduction in the loss of preload (shown in Figure 47).

Figure 47 presents the comparison of loss of preload (%) in the bolts at different clamping lengths. The German design guideline for bolted connections (VDI 2201-1 [28]) was used to estimate the loss of load due to transverse contraction of plate in shear and setting effect of the surfaces.

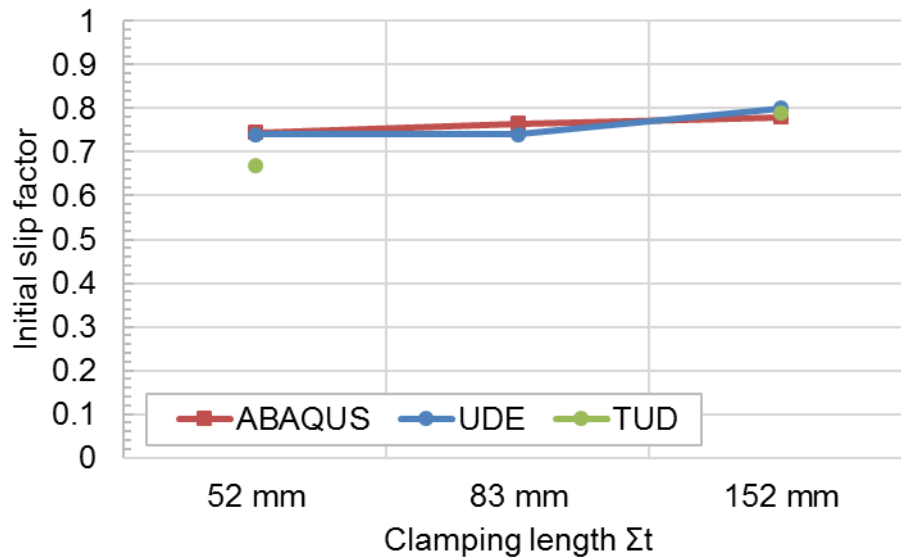


Figure 46 Influence of clamping length on initial slip factor

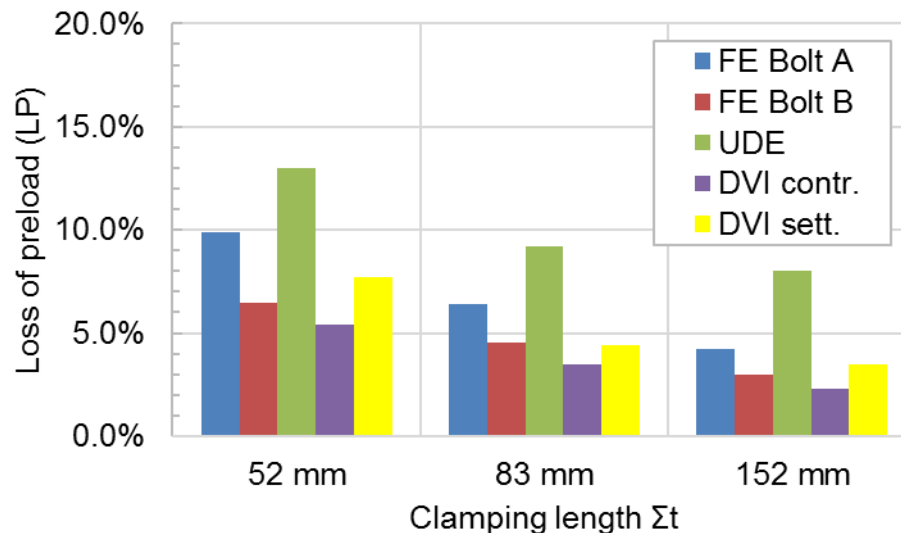


Figure 47 Influence of clamping length on loss of preload (during the slip test)

It can be seen from Figure 47 that both the numerical model and VDI guidelines predicted the correct trend: the loss of preload decreases with increasing clamping length. However, the magnitude of loss of preload from the numerical model and VDI guidelines are smaller than that measured in the UDE test.

The reason is that the numerical model does not consider the setting effect (embedment of contact surfaces). The loss of preload measured in the actual slip test was probably due to a combined effect of contraction and setting. A more favourable agreement can be obtained between the VDI prediction and UDE test if the loss of preload due to contraction and setting calculated using the VDI guidelines are added together.

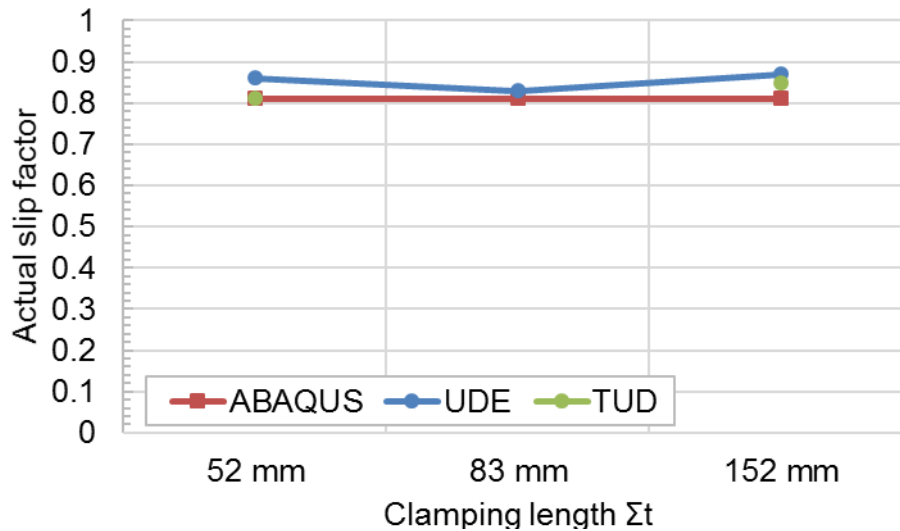


Figure 48 Influence of clamping length on actual slip factor

Finally, the actual slip factors predicted by Abaqus and measured by UDE and TUD are compared in Figure 48. It can be observed from the comparison that the clamping length does not have significant effect on the actual slip factors, which is possibly due to the fact that although the slip load increased with longer clamping length, the loss of preload decreased (i.e. the actual bolt preload at a slip of 0.15 mm increased as well). As a result, the actual slip factor remains relatively constant.

It can be noticed that the actual slip factors predicted by Abaqus are slightly smaller than those measured by UDE and TUD. This is because of a smaller reduction in preload (i.e. higher actual preload load at slip) occurred in the numerical model thus leading to smaller actual slip factors.

8.4.4 Summary

Numerical models of standard slip connection tests of carbon steel (S355, M20 HV 10.9) have been validated against test results from both UDE and TUD. Initial slip factors predicted by the numerical models compared reasonably well with the test results assuming the coefficient of friction $\mu_{fric} = 0.817$ in Abaqus for a grit blasted surface of carbon steel (GB, S355). This compares with the measured values of between 0.48 – 0.55. Prediction of loss of preload and thus actual slip factors by the numerical model is less accurate mainly due to the inability of modelling setting effect in Abaqus, which leads to a smaller preload loss in the numerical model compared with the UDE test.

9. Summary

- Several versions of numerical models of stainless steel bolt assemblies and the plug-in to generate and analyse them have been developed to be used with Abaqus Standard solver.
- The models to be used in subsequent parametric studies were recommended.
- Material definitions including creep and relaxations are recommended for several steel grades (austenitic, ferritic, duplex and lean duplex plates, and austenitic, duplex and lean duplex bolts). Their parameters were calibrated to the real experiments carried out in SIROCO projects and verified by finite element simulations of simple (one-element) models and models of the whole assembly.

References

- [1] Bouchair, A., Averseng, J. and Abidelah, A. Analysis of the behaviour of stainless steel bolted connections. *Journal of Constructional Steel Research* 2008 11;64(11):1264-1274.
- [2] Kim, J., Yoon, J. and Kang, B. Finite element analysis and modelling of structure with bolted joints. *Applied Mathematical Modelling* 2007, 5, Vol. 31, No. 5, pp. 895-911.
- [3] Pavlović, M., Heistermann, C., Veljković, M., Pak, D., Feldmann, M., Rebelo, C. and da Silva, L. Connections in towers for wind converters, part I: Evaluation of down-scaled experiments, *Journal of Constructional Steel Research*, vol. 115, December 2015, pp. 445-457.
- [4] Lorenz, C. and Stranghöner, N., Numerische Simulation des Anziehverhaltens von Schraubverbindungen unter Berücksichtigung des plastischen Materialverhaltens. *Stahlbau*, 85, 2016, pp. 451–458
- [5] Ju, S., Fan, C. and Wu, G.H. Three-dimensional finite elements of steel bolted connections. *Engineered Structures* 2004 2;26(3), pp. 403-413.
- [6] Bursi, O.S., Jaspart, J.P. Benchmarks for finite element modelling of bolted steel connections. *Journal of Constructional Steel Research* 1997 July–September 1997;43(1), pp. 17-42.
- [7] Krolo, P., Grandić, D. and Bulić, M., The Guidelines for Modelling the Preloading Bolts in the Structural Connection Using Finite Element Methods, *Journal of Computational Engineering*, vol. 2016, 8 p.
- [8] You, Q.M., Zhou, H.L., Finite Element Study on Pre-Tightening Process of Threaded Connection and Failure Analysis for Pressure Vessel, *Procedia Engineering* 130 2015, pp. 1385-1396.
- [9] Izumi, S., Yokoyama, T., Iwasaki, A., Sakai, S. Three-dimensional finite element analysis of tightening and loosening mechanism of threaded fastener, *Engineering Failure Analysis* 12 2005, pp. 604–615.
- [10] Python 2.7.12 documentation, accessed online at <https://docs.python.org/2/>
- [11] Hibbit, D., Karlsson, B., Sorensen, P. Abaqus 6.14 Documentation, Online documentation, Dassault Systems, 2014.

- [12] Hibbit, D., Karlsson, B., Sorensen, P. Abaqus 6.14 Scripting Reference Guide, Online documentation, Dassault Systems, 2014.
- [13] Pilhagen, J. SIROCO Deliverable D5.4: Report on tensile and relaxation testing of bar material and bolts
- [14] Fukuoka, T., Nomura, M., Proposition of Helical Thread Modeling With Accurate Geometry and Finite Element Analysis, ASME Journal of Pressure Vessel Technology, vol. 130, February 2008, pp. 011204-1 - 011204-6.
- [15] Hibbit, D., Karlsson, B., Sorensen, P. Abaqus 6.14 Abaqus/CAE User's Guide, Online documentation, Dassault Systems 2014.
- [16] Hibbit, D., Karlsson, B., Sorensen, P. Abaqus 6.14 Keywords Reference Guide, Online documentation, Dassault Systems 2014.
- [17] Gupta I. and Li J. C. M.: Stress relaxation, internal stress, and work hardening in some Bcc metals and alloys, Metall Trans., vol. 1, August 1970, pp. 2323–30.
- [18] Hannula S.-P., Korhonen M.A. and Li C.-Y. : Strain aging and load relaxation behaviour of type 316 stainless steel at room temperature, Metallurgical Transactions A, Vol 17A, October 1986, pp. 1757-1767.
- [19] Holmquist, J.L. and Nadai, A. A theoretical and experimental approach to the problem of collapse of deep-well casing. Drilling and Production Practice 1939, pp. 392-420.
- [20] Ramberg, W. and Osgood, W.R. Technical Note No. 902: Description of stress-strain curves by three parameters. Washington, D.C., USA: National Advisory Committee for Aeronautics, 1943.
- [21] Hill, H.N. Technical Note No. 927: Determination of stress-strain relations from "offset" yield strength values. Washington, D.C., USA: National Advisory Committee for Aeronautics, 1944.
- [22] Mirambell, E. & Real, E. On the calculation of deflections in structural stainless steel beams: an experimental and numerical investigation. Journal of Constructional Steel Research 2000, 4, Vol. 54, No. 1, pp. 109-133.
- [23] Rasmussen, K.J.R. Full-range stress–strain curves for stainless steel alloys. Journal of Constructional Steel Research 2003, 1, Vol. 59, No. 1, pp. 47-61.
- [24] Gardner, L. & Ashraf, M. Structural design for non-linear metallic materials. Engineering Structures 2006, 5, Vol. 28, No. 6, pp. 926-934.
- [25] European Commission for Standardization (CEN), EN 1993-1-4: Eurocode 3 - Design of steel structures - Part 1-4: General rules: Supplementary rules for stainless steels, 1996.
- [26] Manninen, T. SIROCO Deliverable 5.1: Report on available material data and tensile and relaxation testing of the plate material, Outokumpu Stainless Oy, 2017.
- [27] Execution of steel structures and aluminium structures, Part 2: Technical requirements for steel structures, BS EN 1090-2:2008+A1:2011, BSI, 2011.
- [28] Design guidance VDI 2230-1 Systematic calculation of high duty bolted joints – joints with one cylindrical bolt, February 2003.

Annex A: List of model parameters

Table 14. Model parameters used by the script

Parameter	Description	default	plug-in
aSystem	Assembly system	None	2D, 3D
b	Model width in mm	50.0	2D, 3D
bE	Modulus of elasticity of the bolt (if bProp = Custom, GPa)	210.0	-
bISO	Bolt ISO standard (will be assigned according to bStyle)	None	-
bLength	Definition of the bolt length (mm or Automatic)	Automatic	-
bMat	Material type/class of the bolt (if bProp = Custom)	NO PLASTICIT Y	-
bPar	Material parameters of the bolt (if bProp = Custom)		-
bProp	Bolt class (from the library or Custom)	10.9	2D, 3D
bRig	Rigid bolt (True or False)	False	-
bStyle	Bolt style (Bolt (ISO 4014) or Screw (ISO 4017))	Screw (ISO 4017)	2D, 3D
bType	Bolt size (M12 to M30 or Custom)	M16	2D, 3D
bolt Number	Number of bolts in a row (only 3D models)	2	3D
bolt Spacing	Distance between bolts (only 3D models, mm)	50.0	3D
cSize	Mesh size in corners (mm)	0.5	2D, 3D
cb	Distance c of the bolt (if bType = Custom, mm)	0.4	-
cn	Distance c of the nut (if nType = Custom, mm)	0.4	-
d	Bolt diameter (if bType = Custom, mm)	16.0	-
d0	Hole clearance (if hType = Custom, mm)	17.0	-
d1	Washer inner diameter under the nut (if wType = Custom, mm)	17.0	-
d1b	Washer inner diameter under the bolt head (if wType = Custom, mm)	17.0	-
d2	Washer outer diameter under the nut (if wType = Custom, mm)	30.0	-
d2b	Washer outer diameter under the bolt head (if wType = Custom, mm)	30.0	-
dab	Distance d_a of the bolt (if bType = Custom, mm)	16.0	-

dan	Distance d_a of the nut (if nType = Custom, mm)	16.0	-
dim	Model dimensionality (2 or 3)	2	-
dwb	Distance d_w of the bolt (if bType = Custom, mm)	22.0	-
dwn	Distance d_w of the nut (if nType = Custom, mm)	22.0	-
frames Preload	Minimum increments in tightening step(s)	20	2D, 3D
frames Relaxation	Minimum increments in relaxation step(s)	20	2D, 3D
frames Slip	Minimum increments in slip loading step(s)	20	3D
h	Washer height under the nut (if wType = Custom, mm)	0	-
hType	Hole clearance (Fine, Medium, Coarse, None)	Medium	2D, 3D
hb	Washer height under the bolt head (if wType = Custom, mm)	0	-
helix	Generate helical thread in 3D models (True or False)	False	-
k	Bolt head height (if bType = Custom, mm)	6.8	-
l	Length of the shank (if bLength = Custom, mm)	50.0	-
lg	Distance from the bearing face to the first full form full profile thread of the bolt (if bLength = Custom, mm)	0.0	-
load Speed	Preloading speed (RPM)	10.0	2D, 3D
load Together	Preload all the bolts at the same time (True or False)	False	3D
loadWith Deformation	Use always displacement control when force or stress is requested (True or False)	True	-
ls	Length of unthreaded shank (if bLength = Custom, mm)	0.0	-
m	Nut height (if nType = Custom, mm)	14.8	-
mRun	Calculation submission mode (Create only model, Run calculation on local computer, Run calculation on remote server)	Create only model	2D, 3D
mSize	Mesh basic size (mm)	1.5	2D, 3D
nE	Modulus of elasticity of the nut (if nProp = Custom, GPa)	210.0	-

nISO	Nut ISO standard (will be assigned according to nStyle)	None	-
nMat	Material type/class of the nut (if nProp = Custom)	NO PLASTICIT Y	-
nPar	Material parameters of the nut (if nProp = Custom)		-
nProp	Nut class (from the library or Custom)	10	2D, 3D
nRad	Radius of corners in the nut model (mm)	0.0	-
nRig	Rigid nut (True or False)	False	-
nType	Nut style (Style 1 (EN ISO 4032), Style 2 (EN ISO 4033), HR (EN 14399-3), HV (EN 14399-4))	Style 1 (EN ISO 4032)	2D, 3D
overload	Overload of the tightening test step (to estimate deformation needed to achieve certain load)	2.0	2D, 3D
pE	Modulus of elasticity of the plates (if pProp = Custom, GPa)	210.0	-
pMat	Material type/class of the plates (if pProp = Custom)	NO PLASTICIT Y	-
pPar	Material parameters of the plates (if pProp = Custom)		-
pProp	Plates material (from the library or Custom)	Custom	2D, 3D
pRad	Radius of corners in the plates model (mm)	0.0	-
pRig	Rigid plates (True or False)	False	-
pRough1	Roughness of the inner plate (mm)	0.0	2D, 3D
pRough2	Roughness of the outer plate (mm)	0.0	2D, 3D
preload Type	Preload type	BoltLoad	-
rMag1	Relaxation step 1 duration	50.0	2D, 3D
rMag2	Relaxation step 2 duration	0.0	2D, 3D
rMag3	Relaxation step 3 duration	0.0	2D, 3D
rUni1	Relaxation step 1 duration units (seconds, minutes, hours, days, years)	years	2D, 3D
rUni2	Relaxation step 1 duration units (seconds, minutes, hours, days, years)	years	2D, 3D
rUni3	Relaxation step 1 duration units (seconds, minutes, hours, days, years)	years	2D, 3D
rsDir	Remote directory for the remote solver		2D, 3D
rsHost	username@hostname for the remote solver		2D, 3D
rsRS	Location of RemoteSolver.exe		2D, 3D
rsSub	Location of Fortran subroutine		2D, 3D
sMag1	Slip loading magnitude 1	0.0	3D

sMag2	Slip loading magnitude 2	0.0	3D
sMag3	Slip loading magnitude 3	0.0	3D
sUni1	Slip loading units 1		3D
sUni2	Slip loading units 2		3D
sUni3	Slip loading units 3		3D
sb	Distance s of the bolt (if bType = Custom, mm)	24.0	-
sn	Distance s of the nut (if nType = Custom, mm)	24.0	-
t1	Thickness of inner plate (mm)	16.0	2D, 3D
t2	Thickness of outer plate (mm)	8.0	2D, 3D
tMag1	Bolt tightening magnitude 1	70.0	2D, 3D
tMag2	Bolt tightening magnitude 2	0.0	2D, 3D
tMag3	Bolt tightening magnitude 3	0.0	2D, 3D
tUni1	Bolt tightening units 1	% of fy	2D, 3D
tUni2	Bolt tightening units 2	% of fy	2D, 3D
tUni3	Bolt tightening units 3	% of fy	2D, 3D
thread	Modelling threads in 2D and 3D models (True or False)	False	2D, 3D
w	Plates depth (mm)	50.0	3D
wE	Modulus of elasticity of the washers (if wProp = Custom, GPa)	210.0	-
wISO	Washers ISO standard	None	-
wMat	Material type/class of the washers (if wProp = Custom)	NO PLASTICIT Y	-
wPar	Material parameters of the washers (if wProp = Custom)		-
wProp	Washer material (from the library or Custom)	Custom	2D, 3D
wRad	Radius of corners in the washers model (mm)	0.0	-
wRig	Rigid washers	False	-
wRough	Roughness of washers surface	0.0	-
wType	Washer series (Normal (EN ISO 7091), Large (EN ISO 7093-1), HR/HV (EN 14399-5))	Normal (EN ISO 7091)	2D, 3D
xSymm	Vertical transverse symmetry plane in 3D models (True or False)	False	-
ySymm	Horizontal symmetry plane (True or False)	False	2D, 3D
P	Thread pitch (if bProp = Custom, mm)	2.0	-

Annex B: Material library

The definition of elastic and inelastic behaviour (including creep and relaxation) takes usually many parameters, and therefore a library of pre-defined materials was developed. The material is there defined by 3-letter material code and a sequence of parameters. The codes, parameters and default materials are explained in the following tables.

Table 15. Material codes

Material code	Model type	parameters
PLA	ideally plastic material	Modulus of elasticity, Yield strength E, f_y
BLN	bi-linear plasticity	Modulus of elasticity, Yield strength Ultimate strength and strain E, f_y f_u, ϵ_u
HNA	Holmquist - Nadai [19]	Modulus of elasticity, Yield strength E, f_y Proportional limit stress and strain f_p, ϵ_y Nonlinearity n
SRO	Ramberg-Osgood [20] Hill [21]	Modulus of elasticity, 0.2% proof stress $E, \sigma_{0.2}$ Nonlinearity n
MRO	Mirambell-Real [22]	Modulus of elasticity, 0.2% proof stress $E, \sigma_{0.2}$ Ultimate strength and strain f_u, ϵ_u 1 st and 2 nd nonlinearity n, m
RRO	Rasmussen [23]	Modulus of elasticity, 0.2% proof stress $E, \sigma_{0.2}$ Nonlinearity n
GRO	Gardner [24]	Modulus of elasticity, 0.2% proof stress $E, \sigma_{0.2}$ 1% proof stress $\sigma_{1.0}$ 1 st and 2 nd nonlinearity n, m
SRC	SRO with CREEP subroutine	Modulus of elasticity, 0.2% proof stress $E, \sigma_{0.2}$ Nonlinearity n CREEP parameters a, b, c_1, c_2, c_3
MRC	MRO with CREEP subroutine	Modulus of elasticity, 0.2% proof stress $E, \sigma_{0.2}$ Ultimate strength and strain f_u, ϵ_u 1 st and 2 nd nonlinearity n, m CREEP parameters a, b, c_1, c_2, c_3
RRC	RRO with CREEP subroutine	Modulus of elasticity, 0.2% proof stress $E, \sigma_{0.2}$ Nonlinearity n CREEP parameters a, b, c_1, c_2, c_3
GRC	GRO with CREEP subroutine	Modulus of elasticity, 0.2% proof stress $E, \sigma_{0.2}$ 1% proof stress $\sigma_{1.0}$ 1 st and 2 nd nonlinearity n, m CREEP parameters a, b, c_1, c_2, c_3
UHA	Mixed isotropic and kinematic hardening with UHARD subroutine	Modulus of elasticity, Yield strength E, f_y Number of backstresses N Backstress components $C_1, \gamma_1 \dots C_N, \gamma_N$ UHARD parameters D, n, Q, b, k
CUS	Custom model	parameters will be defined manually in GUI

Table 16. Pre-defined material models

Material identification(s)	Code	E	Parameters	Restriction
1.4003 3Cr12, S41003, S40977, 409L	SRO	220 GPa	$\sigma_{0.2}=280$ MPa, $n=7$, $f_u=450$ MPa	plate washer
1.4016 S43000, 430	SRO	220 GPa	$\sigma_{0.2}=260$ MPa, $n=6$, $f_u=450$ MPa	plate washer
1.4512 X2CrTi12, S40900, 409	SRO	220 GPa	$\sigma_{0.2}=210$ MPa, $n=9$, $f_u=380$ MPa	plate washer
1.4306, 1.4307, 1.4541 S30403, S32100, 304L, 321	SRO	200 GPa	$\sigma_{0.2}=220$ MPa, $n=6$, $f_u=520$ MPa	plate washer
1.4301 S30400, 304	SRO	200 GPa	$\sigma_{0.2}=230$ MPa, $n=6$, $f_u=540$ MPa	plate washer
1.4401, 1.4404, 1.4539 S31600, S31603, 316, 316L	SRO	200 GPa	$\sigma_{0.2}=240$ MPa, $n=7$, $f_u=530$ MPa	plate washer
1.4539 N08904, 904L	SRO	195 GPa	$\sigma_{0.2}=240$ MPa, $n=7$, $f_u=530$ MPa	plate washer
1.4571 S31635, 316Ti	SRO	200 GPa	$\sigma_{0.2}=240$ MPa, $n=7$, $f_u=540$ MPa	plate washer
1.4432, 1.4435	SRO	200 GPa	$\sigma_{0.2}=240$ MPa, $n=7$, $f_u=550$ MPa	plate washer
1.4311 S30453, 304LN	PLA	200 GPa	$f_y=300$ MPa	plate washer
1.4439 317LMN, S31726	PLA	200 GPa	$f_y=290$ MPa	plate washer
1.4529 N08926, 926	PLA	195 GPa	$f_y=300$ MPa	plate washer
1.4547 S31254,254SMO	PLA	195 GPa	$f_y=320$ MPa	plate washer
1.4318 301LN, S30100	SRO	200 GPa	$\sigma_{0.2}=350$ MPa, $n=6$, $f_u=650$ MPa	plate washer
1.4362 S32304	SRO	200 GPa	$\sigma_{0.2}=420$ MPa, $n=5$, $f_u=600$ MPa	plate washer
1.4462 S32205, 2205, S31803, 318LN	SRO	200 GPa	$\sigma_{0.2}=480$ MPa, $n=5$, $f_u=660$ MPa	plate washer
S235	PLA	210 GPa	$f_y=235$ MPa	plate washer

S278	PLA	210 GPa	$f_y=275$ MPa	plate washer
S355	PLA	210 GPa	$f_y=355$ MPa	plate washer
S460	PLA	210 GPa	$f_y=460$ MPa	plate washer
S700	PLA	210 GPa	$f_y=700$ MPa	plate washer
S960	PLA	210 GPa	$f_y=960$ MPa	plate washer
PLATE 1.4404, PLATE 316L	UHA	200 GPa	see <i>Table 6</i> and <i>Table 7</i>	plate washer
PLATE 1.4003 PLATE 410L	UHA	200 GPa	see <i>Table 6</i> and <i>Table 7</i>	plate washer
PLATE 1.4462 PLATE 2205	UHA	200 GPa	see <i>Table 6</i> and <i>Table 7</i>	plate washer
PLATE 1.4162 PLATE 2101	UHA	200 GPa	see <i>Table 6</i> and <i>Table 7</i>	plate washer
BOLT 1.4401 BOLT 316	MRC	200 GPa	see <i>Table 3</i> and <i>Table 5</i>	bolt nut
BOLT 1.4162 BOLT 2101	MRC	200 GPa	see <i>Table 3</i> and <i>Table 5</i>	bolt nut
BOLT 1.4162 BOLT 2101	MRC	200 GPa	see <i>Table 3</i> and <i>Table 5</i>	bolt nut
45, F1	PLA	220 GPa	$f_y=450$ MPa	bolt
50, A1, A2	PLA	200 GPa	$f_y=500$ MPa	bolt
60, F2	PLA	220 GPa	$f_y=600$ MPa	bolt
70, A3, A4	PLA	200 GPa	$f_y=700$ MPa	bolt
80, A5	PLA	200 GPa	$f_y=800$ MPa	bolt
8.8	PLA	210 GPa	$f_y=640$ MPa	bolt
10.9	PLA	210 GPa	$f_y=900$ MPa	bolt
6	PLA	210 GPa	$f_y=600$ MPa	nut
8	PLA	210 GPa	$f_y=800$ MPa	nut
10	PLA	210 GPa	$f_y=1000$ MPa	nut

Annex C: Configuration file example

```
#####  
# SIROCO CONFIGURATION FILE #  
# by VTT Technical Research Centre of Finland #  
# 2014-2016 #  
#####  
  
*** General information ***  
mName='BOLT_ASSEMBLY_3D1B3TH' # Model name  
mDim='3' # Model dimensionality  
boltNumber=1 # Number of bolts in a row (only 3D models)  
boltSpacing=50 # Distance between bolts (only 3D models)  
  
*** Standardized parameters ***  
bType='M16' # Bolt size  
bStyle='Screw (ISO 4017)' # Bolt style  
bProp='UHARD bolt' # Bolt class  
nType='Style 1 (EN ISO 4032)' # Nut style  
nProp='UHARD bolt' # Nut class  
wType='Normal (EN ISO 7091)' # Washer series  
wProp='UHARD plate' # Washer material  
pProp='UHARD plate' # Plates material  
hType='Medium' # Hole clearance  
  
*** Bolt properties ***  
l=50.0 # Length of the shank  
lg=0.0 # Distance from the bearing face to the first full form (full  
profile) thread (bolt)  
ls=0.0 # Length of unthreaded shank  
  
*** Washer properties ***  
d1b=17.0 # Washer inner diameter (under the bolt head)  
d2b=30.0 # Washer outer diameter (under the bolt head)  
hb=0 # Washer height (under the bolt head)  
  
*** Plates properties ****  
t1=16 # Thickness of inner plate  
t2=8 # Thickness of outer plate  
d0=17 # Hole clearance  
b=100 # Model width  
w=100 # Model depth  
  
*** Loading parameters ***  
loadSpeed=10 # Preloading speed  
overload=4 # Overload of the tightening test step (to estimate  
deformation needed to achieve certain load)  
framesPreload=200 # Minimum increments in tightening step(s)  
framesSlip=20 # Minimum increments in slip loading step(s)  
framesRelaxation=20 # Minimum increments in relaxation step(s)
```

*** Loading pattern ***

loadTogether=False # Preload all the bolts at the same time

lMag1

lUni1

sMag1=0

sUni1='kN'

rMag1=5

rUni1='years'

lMag2

lUni2

sMag2=0

sUni2='kN'

rMag2=5

rUni2='years'

lMag3

lUni3

sMag3=0

sUni3='kN'

rMag3=40

rUni3='years'

*** Other ***

P=2.0

bE=210.0

bLength='Automatic' # Definition of bolt length

bRig=False

cSize=0.15

dim=2

helix=False

loadWithDeformation=True # Use always displacement control when
force or stress is requested

mRun='Create only model'

mSize=0.6

nE=210.0

nRad=0.0

nRig=False

pE=210.0

pRad=0.0

pRig=False

pRough1=0

pRough2=0

tMag1=70

tMag2=70

tMag3=70

tUni1='% of fy'

tUni2='% of fy'

tUni3='% of fy'

thread=True

wE=210.0

wRad=0.0

wRig=False

wRough=0.0

xSymm=False

ySymm=True

Annex D: CREEP subroutine

by Merja Sippola and Anssi Laukkanen, December 2015

```
      SUBROUTINE CREEP(DECRA,DESWA,STATEV,SERD,EC,ESW,P,QTILD,
&  TEMP,DTEMP,PREDEF,DPRED,TIME,DTIME,CMNAME,LEXIMP,LEND,
&  COORDS,NSTATV,NOEL,NPT,LAYER,KSPT,KSTEP,KINC)
      INCLUDE 'ABA_PARAM.INC'
      CHARACTER*80 CMNAME
      DIMENSION DECRA(5), DESWA(5), STATEV(*), PREDEF(*), DPRED(*)
      DIMENSION TIME(3), EC(2), ESW(2), COORDS(*)
      i1=0
      do i1=1,5
         DECRA(i1)=0
         DESWA(i1)=0
      end do
      IF (LEND==0) THEN
         CTIME=TIME(1)-DTIME
      ELSE IF (LEND==1) THEN
         CTIME=TIME(1)
      END IF
      IF ((QTILD .GT. STATEV(5)) .AND. (QTILD .GE. 1.0d0)) THEN
         STATEV(5)=QTILD
         STATEV(6)=CTIME
         SIGMA0=QTILD
         TIME0=CTIME
      ELSE
         SIGMA0=STATEV(5)
         TIME0=STATEV(6)
      END IF
      c11 = <material parameter c1>
      c12 = <material parameter c2>
      c13 = <material parameter c3>
      cc = c11*SIGMA0*SIGMA0+c12*SIGMA0+c13
      Xn = <material parameter n>
      XE = <modulus of elasticity in MPa>
      AA = <material parameter a>
      IF (QTILD .GE. 1.0d0) THEN
         Xker1 = (Xn/(Xn-1.0d0))
         Xker2 = (1.0d0-Xn)
         Xker3 = Xker2/cc
         DEC = Xker3*EC(1)+(AA**Xker2)
         DECRA(1)=(cc*(DEC**Xker1))*DTIME
         STATEV(1) = DECRA(1)
      ELSE
      END IF
      RETURN
      END
```

Annex E: UHARD subroutine

by Timo Manninen, 30.6.2015

```
SUBROUTINE UHARD(SYIELD,HARD,EQPLAS,EQPLASRT,TIME,DTIME,TEMP,
$      DTEMP,NOEL,NPT,LAYER,KSPT,KSTEP,KINC,
$      CMNAME,NSTATV,STATEV,NUMFIELDV,
$      PREDEF,DPREDEF,NUMPROPS,PROPS)
  INCLUDE 'ABA_PARAM.INC'
  CHARACTER*80 CMNAME
  PARAMETER (ONE=1.0D0, ZERO=0.0D0)
  DIMENSION HARD(3),STATEV(NSTATV),TIME(*),
$          PREDEF(NUMFIELDV),DPREDEF(*),PROPS(*)
  Q      = PROPS(1)
  B      = PROPS(2)
  SIG0   = PROPS(3)
  PK     = PROPS(4)
  PN     = PROPS(5)
  RATE0  = PROPS(6)
  PNINV  = ONE / PN
  PNINVM1 = PNINV - ONE
  PLTERM = SIG0 + Q * (ONE - EXP(-B*EQPLAS))
  PLDERI = Q * B * EXP(-B*EQPLAS)
  IF (EQPLASRT.GE.RATE0) then
    RADERI = PNINV * PK * (EQPLASRT**PNINVM1)
    RATERM = PK * (EQPLASRT**PNINV)
  ELSE
    RADERI = PNINV * PK * (RATE0**PNINVM1)
    RATERM = PK * (RATE0**PNINV) - RADERI*(RATE0 - EQPLASRT)
  ENDIF
  SYIELD = PLTERM + RATERM
  HARD(1) = PLDERI
  HARD(2) = RADERI
  HARD(3) = ZERO
  RETURN
END
```

Annex E: UAMP subroutine

by Petr Hradi and Anqi Chen 14.6.2016

```
SUBROUTINE UAMP(
*   ampName, time, ampValueOld, dt, nProps, props, nSvars,
*   svars, lFlagsInfo,
*   nSensor, sensorValues, sensorNames, jSensorLookUpTable,
*   AmpValueNew,
*   lFlagsDefine,
*   AmpDerivative, AmpSecDerivative, AmpIncIntegral,
*   AmpDoubleIntegral)
INCLUDE 'ABA_PARAM.INC'
dimension sensorValues(nSensor), svars(nSvars), PROPS(nProps)
character*80 sensorNames(nSensor)
character*80 ampName
character*80 sensorName
PARAMETER (ONE=1.0D0, ZERO=0.0D0, MULTI=1.0D0)
parameter (iStepTime      = 1,
*          iTotTime       = 2,
*          nTime           = 2)
parameter (iInitialization = 1,
*          iRegularInc     = 2,
*          iCuts           = 3,
*          ikStep          = 4,
*          nFlagsInfo      = 4)
parameter (iComputeDeriv  = 1,
*          iComputeSecDeriv = 2,
*          iComputeInteg   = 3,
*          iComputeDoubleInteg = 4,
*          iStopAnalysis   = 5,
*          iConcludeStep   = 6,
*          nFlagsDefine    = 6)
dimension time(nTime), lFlagsInfo(nFlagsInfo),
*          lFlagsDefine(nFlagsDefine)
dimension jSensorLookUpTable(*)
      SENS = PROPS(1)
RATE = PROPS(2)
      FPC = PROPS(3)
      write(sensorName,'(A,I1)') 'FORCE-SENSOR-',INT(SENS)
force_sensor = GetSensorValue(sensorName,
*                               jSensorLookUpTable,
*                               sensorValues)
if (lFlagsInfo(iInitialization).eq.1) then
  ampValueNew = ampValueOld + MULTI*RATE*dt
  lFlagsDefine(iConcludeStep) = 0
else
  ampValueNew = ampValueOld + MULTI*RATE*dt
  if (force_sensor .gt. FPC) then
    lFlagsDefine(iConcludeStep) = 1
  end if
end if
RETURN
END
```

Annex F: Derivation of strain-hardening model

This Annex explains in detail the conversion of time-hardening model (Eq. (5)) to strain-hardening model (Eq. (6)).

From Gupta et al. [17]:

$$\dot{\varepsilon}_v = c(t + a)^{-b}$$

In relaxation test, the elastic strain rate cancels to the creep strain rate, and therefore

$$\dot{\varepsilon}_v = -\frac{1}{E}\dot{\sigma} = -\frac{1}{E}\frac{d\sigma}{dt}$$

By combining previous two equations we can get stress rate

$$\begin{aligned}\frac{d\sigma}{dt} &= -Ec(t + a)^{-b} \\ d\sigma &= -Ec(t + a)^{-b} dt\end{aligned}$$

The stress function can be integrated by substitution

$$\int_{\sigma_0}^{\sigma} d\sigma = \int_{\sigma(t_0=0)}^{\sigma(t)} d\sigma = \int_0^t -Ec(t + a)^{-b} dt$$

And then

$$\begin{aligned}\sigma - \sigma_0 &= \int_0^t \frac{1}{1-n} \cdot Ec(t + a)^{1-b} = -\frac{Ec}{(1-n)} [(t + a)^{1-b} - (0 + a)^{1-b}] = -\frac{Ec}{(1-n)} [(t + a)^{1-b} - a^{1-b}] \\ \sigma &= \sigma_0 - \frac{Ec}{(1-n)} [(t + a)^{(1-b)} - a^{(1-b)}]\end{aligned}$$

Also as

$$\begin{aligned}\dot{\varepsilon}_v &= \frac{d\varepsilon_v}{dt} = c(t + a)^{-b} \\ \varepsilon_v &= \int_0^t c(t + a)^{-b} dt = \frac{c}{(1-b)} (t + a)^{(1-b)} - \frac{c}{(1-b)} a^{1-b}\end{aligned}$$

So

$$\dot{\varepsilon}_v = c(t + a)^{-b} = \frac{c}{1-b} (t + a)^{(1-b)} (1-b)(t + a)^{-1}$$

Now

$$(t + a)^{(1-b)} = \frac{(1-b)}{c} \dot{\varepsilon}_v + a^{(1-b)}$$

Thus

$$(t + a) = \left[\frac{(1-b)}{c} \varepsilon_v + a^{(1-b)} \right]^{\frac{1}{(1-b)}}$$

And finally

$$\dot{\varepsilon}_v = c \left[\left[\frac{(1-b)}{c} \varepsilon_v + a^{(1-b)} \right]^{\frac{1}{(1-b)}} \right]^{-b} = c \left[\frac{(1-b)}{c} \varepsilon_v + a^{(1-b)} \right]^{\frac{b}{(b-1)}}$$